JOURNAL OF SOLID STATE CHEMISTY 1, 237–267 (1970)

A Systematic Survey of Cubic Crystal Structures

A. L. LOEB

Ledgemont Laboratory, Kennecott Copper Corporation, Lexington, Massachusetts 02173

Received September 10, 1969

Although the close-packed sphere model has been successful in systematically correlating a large variety of crystal structures, it fails to allow for the prevalence of bcc structures, and hence precludes a systematic approach to bcc derivatives. An empirical alternative to the sphere-packing model, the Vector Equilibrium Principle, is proposed, according to which an interstice in any regular array is defined as a vertex of a Dirichlet domain of that array. Accordingly, many cubic crystals are recognized as distortions from idealized patterns which in turn constitute permutations and combinations of a small number of invariant point complexes. These point complexes are substitutional or interstitial derivatives from the bcc lattice.

A. Introduction

The problems encountered in any attempt at systematically classifying crystal structures depend to a large extent on the symmetry of the crystals under consideration. In the triclinic and monoclinic classes we find many idiosyncratic structures whose interrelationships, if any exist, are difficult to discern. On the other hand, in the cubic system it is the multitude and variety of the crystals and the complexity of their interrelations that confound the systematologist. Moreover, the cubic system is the only truly three-dimensional one, the others having at least one unique direction in space. The cubic system therefore requires true three-dimensional visualization, i.e. the ability to visualize the projection of *any* plane when the projection on and elevations out of a single plane are given. Many crystals of lower symmetry may be recognized as distorted forms of cubic structures; it is therefore well to start any attempt at classification at the high-symmetry end.

Systematology is the science or art of arranging entities in a meaningful array such that the relations between them are evident. A structure is an ordered array of entities that bear definite relations to each other. A crystal is an array of atoms or ions whose positions, and possibly orientations, can be determined experimentally. A crystal *structure*, on the other hand, is more than an array of ions or atoms: imaginary lines connecting these elements define spatial relations between them. These lines are conceptual rather than experimentally determinate, hence subjective and subject to controversy.

Systematology likewise is subjective. What is meaningful to some is useless to others, what is obvious in one context is obscure in another. Controversial, for instance, is the question whether a classification of crystals should be based on geometrical considerations only, or on bond types as well. Some consider sphalerite as a substitutional derivative of diamond, while others consider this geometrical relation between diamond and sphalerite fortuitous because the bonding is quite different in the two structures. In many cases, particularly intermetallics, the distinction is not very clear, and geometrical resemblances may be fortuitous, or may be due to some underlying principle. The cations of spinel, for instance, occupy an array identical to that occupied by the metal ions in the Cu_2Mg Laves phase. The former structure may be expressed as a cubic close-packed array of oxide ions with a symmetrical distribution of cations over octahedral and tetrahedral voids, but the latter has no close-packed ions or voids which would determine the position of the metal ions. It is difficult to say definitely if the resemblance between spinel and the Laves phase is fortuitous or based on some significant principle of crystal architecture. In point of fact, the constraints of stoichiometry and symmetry limit the number of possible arrays [Loeb (*1*), Figueiredo (*2*)], and may well dominate bonding

considerations in determining structure. As the applications of systematology frequently lie in areas where details of properties and bond type are not well understood or controversial, this author prefers a system based exclusively on geometry.

Models may be physical, conceptual, or both. A physical model of a crystal presupposes a detailed knowledge of the electronic arrangements and behavior of the crystal. A conceptual model may at times be a conjectural rationalization without physical basis. The use of a conceptual model in systematology is well exemplified by the signs of the zodiac. The lines drawn between stars by astrologers have turned out to be physically meaningless, and the influence of these signs on terrestrial life is, at best, conjectural. Nevertheless, those signs have provided a useful frame of reference to astrologers and astronomers, facilitating the recognition, recording, and communication of celestial data.

The program for this paper is, consecutively: (1) a discussion of significant patterns to look for in cubic crystals, including a generalization of the concept of an interstice, (2) a quantitative description of these patterns and their relationship to each other, (3) the enumeration of some basic arrays which in various permutations and combinations constitute the vast majority of cubic crystals, (4) the recognition of these arrays in data on crystals, and (5) a discussion of actual crystals and their systematic relationships.

B. Sphere Packing

The successful model of closely packed spheres has led to systematic schemes relating a variety of crystal structures (Fig. 1) [Loeb (*3*, *4*), Jellinek (*5*), Morris and Loeb (*6*), Gehman (*7*, *8*, *9*), Lima-de Faria (*10*, *11*), Smirnova (*12*)]. Yet its success may be partly fortuitous: its failure to account for the prevalence of body-centered structures and their derivatives is a shortcoming as a conceptual model. Its failure to account for many alloys, and for such relations as that mentioned between spinel and the Laves Cu_2Mg phase, make the sphere-packing model questionable as a physical model.

The sphere packing model corresponds to an interaction potential such as shown in Fig. 2a. This potential is constant when the distance between the centers of the spheres is greater than the sum of their radii, and infinite when this distance is less than the sum of the radii. A system subject to such interaction potentials is

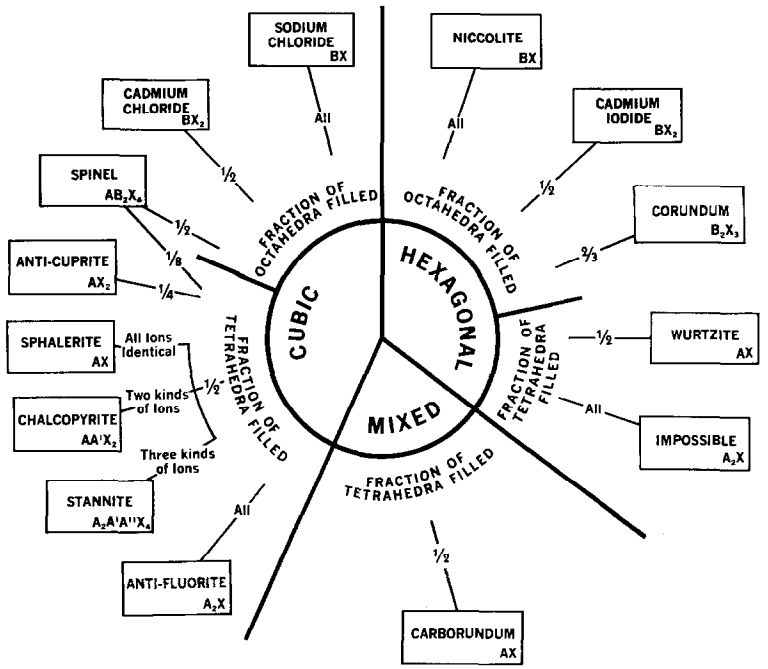

FIG. 1. Systematic arrangement of interstitial derivatives from fcc and hcp complexes.

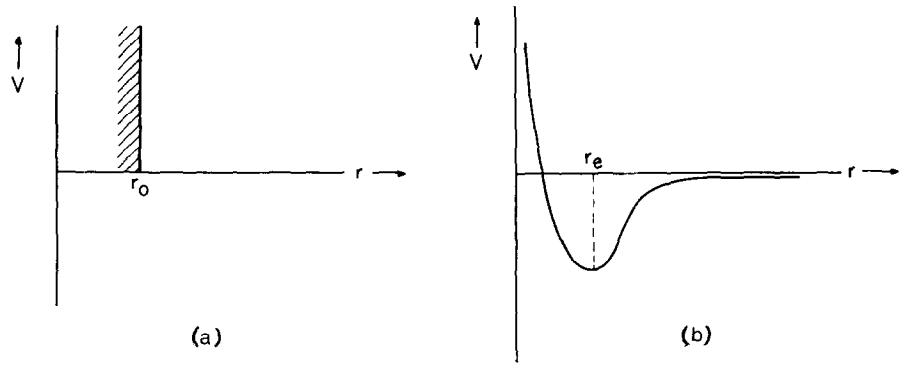

FIG. 2. (a) Interaction potential for rigid spheres. (b) Interaction potential as a function of distance for a stable system.

not stable except under external compression, in which case the only stable configurations are close-packed ones. Actually, a stable configuration requires a potential as shown in Fig. 2b, being repulsive at small distances, attractive at larger distances, and having a minimum at the so-called equilibrium distance. This behavior is true regardless of the detailed nature of the interaction. Before discussing very large systems subject to such interactions, let us consider the behavior of just a few interacting entities.

Two atoms subject to a potential illustrated in Fig. 2b form a diatomic molecule oscillating about the equilibrium distance r_e. Three atoms will arrange themselves at the vertices of an equilateral triangle; the determination whether a stable potential function can exist for three atoms lies in the domain of wave mechanics. It suffices here to state that if such a potential exists, the resulting configuration will be an equilateral triangle.

Four atoms might arrange themselves either at the corners of a square, or at the vertices of a regular tetrahedron. Four entities have $\frac{1}{2}(4 \cdot 3) = 6$ connections between them; for the tetrahedron these six connections are all edges and equal in length. In the square, four of the connections are edges and two are diagonals. Clearly, the tetrahedral arrangement is the more stable one because all connections can be at the equilibrium distance, while for the square either the edges are shorter than the equilibrium distance, and want to expand, or the diagonals are longer and want to contract. The square would therefore tend to buckle and form a tetrahedron (Fig. 3). The stability of the tetrahedron [cf. R. Buckminster Fuller (*13*)] is not due to any particular type of interaction (e.g., corresponding to rigid rods or spheres), but to the tendency for a maximum number of connections to be equal in length to the equilibrium distance. In any configuration consisting of more than four entities (having more than six connections) the connections are necessarily of different lengths, so that a compromise must be struck. With an interaction like that of Fig. 2a, the shortest connections are given unique weight, and the influence of the longer connections is ignored altogether. Therefore, it is not surprising that the sphere-packing model accounts for nothing but the close-packed structures. Figure 2b shows, on the other hand, that all connections play a role in determining an optimum

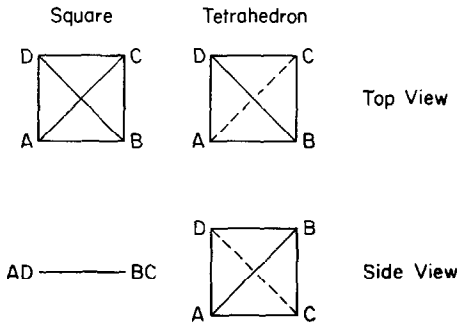

FIG. 3. Connections between four items.

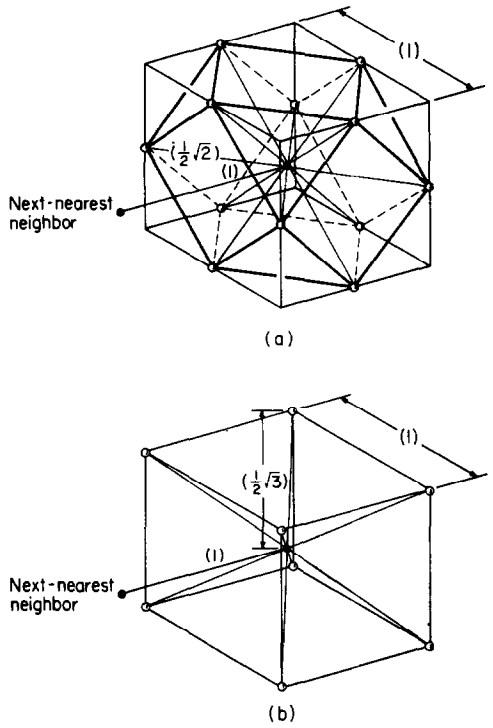

FIG. 4. Comparison of nearest and next-nearest neighbors in the fcc and bcc lattices. (a) fcc: unit cell chosen with its center on a close-packed atom. (b) bcc.

configuration; energetically all connections will tend to equal the equilibrium distance, r_e, but geometrical constraints preclude this situation. Compromises must therefore be struck, in which the distribution of connection distances depends on the exact form of the interaction potential.

In the body-centered configuration there are only eight nearest neighbors, but six next-nearest neighbors only 15% further away (Fig. 4b). By contrast, the face-centered structure has twelve nearest neighbors, with six next-nearest neighbors 41% further away (Fig. 4a). With the proper interaction potential, the relative paucity of nearest neighbors in the bcc structure can be easily compensated for by the proximity of next-nearest neighbors. Different interaction potentials lead to different compromises; the great complexity of many structures, particularly intermetallics, is the result of a delicate balance between various idealized patterns.

C. The Vector Equilibrium Principle

On the basis of the discussion of the previous section an alternate principle to the sphere-packing model is postulated. This principle is phenomenological, and no more profound than the sphere-packing model, but more encompassing. It will, therefore, permit the inclusion of bcc structures and their derivatives together with the fcc structures and derivatives in a single system. Being based on the establishment of equilibrium between attractive and repulsive forces, it will be called the Vector Equilibrium Principle (V.E.P.):

> Crystal structures tend to assume configurations in which a maximum number of identical atoms and ions are equidistant from each other; if more than a single type of atom or ion is present, each atom or ion tends to be equidistant from as many as possible of each type of atoms or ions.

It should be noted that the V.E.P. marks *tendencies*, recognizing the need for compromises in satisfying geometrical and stoichiometrical constraints.

It is of interest to compare the V.E.P. with three principles formulated by Laves (*14*) as a rationale primarily for intermetallics:

a. Space Principle (aiming at efficient space filling),
b. Symmetry Principle (aiming at highest symmetry),
c. Connection Principle (aiming at connections of highest dimension).

Of these three, the second and third are encompassed by the V.E.P.; the Connection Principle is illustrated by the "buckling" of a square to form a tetrahedron. The Space Principle is modified by the V.E.P., because we are dealing with a "soft" interaction (Fig. 2b) rather than with rigid bodies.

D. Dirichlet Domain and Coordination Polyhedron

Frank and Kasper (*15*, *16*) have given a very elegant and rigorous definition of coordination that is independent of mechanical contact between rigid spheres. Consider a regular array of discrete points. A Dirichlet domain for such an array is a region of space within which every point is closer to a given one than to any other of the array of discrete points. When the discrete points are regularly spaced, the Dirichlet domain around each point is congruent with that around every other point, hence is a space-filling polyhedron.

The Dirichlet domain is constructed (cf. Frank and Kasper, op. cit.) by connecting one member of the array to every other member, and perpendicularly bisecting each connection by a plane. The innermost polyhedron enclosed by the bisector planes is the Dirichlet domain. The polyhedron whose vertices are the mirror images of the center of the Dirichlet domain in each of its faces is called the *coordination polyhedron.* To each face of the Dirichlet domain there corresponds a vertex of the coordination polyhedron. This observation led Frank and Kasper to conclude that Dirichlet domain and coordination polyhedron are generally each other's duals. However, since it is *not* generally true that to each face of the coordination polyhedron there corresponds a vertex of the Dirichlet domain, the duality relation is only true in special cases. The duality relation does hold for the fcc lattice, but not for the bcc lattice; we shall see presently that the bcc Dirichlet domain is quite significant in determining the systematic relationship between fcc and bcc derivatives.

E. Interstices

In abandoning the sphere-packing model, we have lost the concept of an interstice, or void, between spheres. The V.E.P. provides that when a second type of ion is introduced into a regular array of ions, this second type of ion must be equidistant from a maximum number of ions of this regular array.

Each face of a Dirichlet domain is part of the locus of all points equidistant from two points in the array. The intersection of two faces, an edge, is equidistant from at least three points in the array, which lie in a plane normal to the edge. The interesection of two edges, namely a vertex of the Dirichlet domain, is equidistant from at least four noncoplanar points of the array. We can accordingly define a general interstice in any regular array as a vertex of a Dirichlet domain of that array. We shall show that this definition is consistent with the concept of an interstice in the close-packed arrays.

F. The fcc Array

In the fcc array the coordination polyhedron is a cuboctahedron (Fig. 5a), which can be inscribed in a cube, its vertices being located at the midpoints of cube edges. It has, therefore, 12 vertices (cf. Fig. 4a). Crystallographers use a cartesian coordinate system in which the origin is at the center of the cube and the x, y, and z axes are parallel to the cube edges; the unit lengths of x, y, and z are chosen equal to the length of the cube edge. The vertices of the cuboctahedron then have the coordinates $\pm(\frac{1}{2}\frac{1}{2}0)$ where $)$ indicates a cyclic permutation, and $\pm$ acts on all coordinates within the parentheses. The author (*3*, *6*) has defined a

hexagonal coordinate system whose h axis is parallel to a body diagonal of the cube, and whose v and w axes are projections of the y and z axes on a plane perpendicular to the body diagonal (a 1 1 1-plane)†:

$$h = 2(x + y + z); \quad v = 6y - h; \quad w = 6z - h.$$

An advantage of this hexagonal coordinate system is that the *entire* infinite fcc array is described by the equations,

$$v \overset{3}{=} 2h; \quad w \overset{3}{=} 2h; \quad h = 2K, \quad \text{where } K \text{ is any integer.}$$

Here the symbol 3 denotes equality modulo − 3, meaning that the difference between the expressions on both sides of the equal sign must be an integral multiple of 3. These hexagonal coordinates are indicated at the vertices of the cuboctahedron in Fig. 5a. The cross section through this polyhedron at $h = 0$ is a hexagon, formed by the close-packing arrangement in a plane. The vertices at $h = \pm 2$ form triangles above and below the hexagonal equator, which are part of a close-packed planar array extending beyond the cubic cell. The hexagonal coordinate system thus naturally fits the close-packed arrays.

The Dirichlet domain of the fcc array is a rhombohedral dodecahedron (Fig. 5b). At six of its vertices four acute angles meet; these we shall call the *acute* vertices. All acute vertices have *odd* values of h. At eight of the vertices three obtuse angles meet; these so-called *obtuse* vertices have *half-integral* values of h. The rhombododecahedron has 12 faces and 14 vertices; from Euler's equation $v - e + f = 2$ (where v =number of vertices, e = number of edges, f = number of faces), it follows that it has 24 edges (cf., for instance, D. Hilbert and S. Cohn-Vossen, "Geometry and the Imagination," Chelsea Publ. Co., N.Y. 1952, p. 290 ff). The cuboctahedron has 14 faces, 12 vertices, and 24 edges. The coordination polyhedron and Dirichlet domain are, in the fcc array, each other's duals. (Since duals have the same value of $v + f$, it follows from Euler's equation that they necessarily have the same number of edges.)

Gorter (*17*) has pointed out in connection with the sphere-packing model that the centers of the interstices surrounding a sphere in a close-packed array constitute the vertices of a rhombododecahedron. Accordingly, the general definition of an interstice as a vertex of a Dirichlet domain agrees with the conventional concept of an interstice in the case of cubically close-packed array of spheres. The acute vertices of the rhombododecahedron correspond to octahedral interstices, and are characterized by odd values of h. The obtuse vertices correspond to tetrahedral interstices, and are characterized by half-integral values of h. The octahedral interstices by themselves constitute the vertices of octahedra around the fcc points. The tetrahedral interstices together form cubes around the fcc points, but they may be subdivided into two interpenetrating sets each of which separately forms tetrahedra around the fcc points. These two sets of tetrahedra are distinguished from each other by their values of h: for one set h equals an even number *minus* $\frac{1}{2}$, while for the

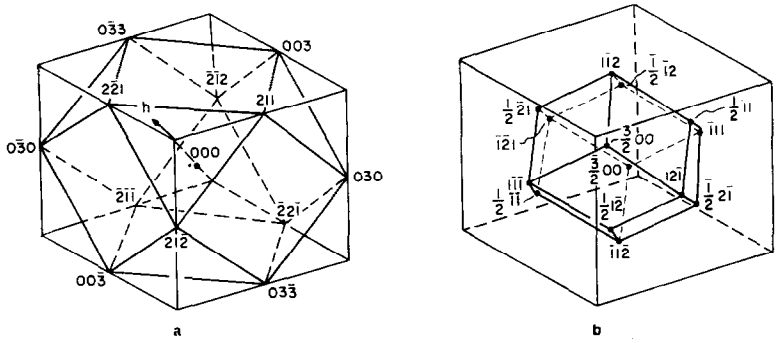

FIG. 5. (a) Coordination polyhedron of the fcc array: cuboctahedron. (b) Dirichlet domain of the fcc array: rhombohedral dodecahedron. Coordinates shown are h, v, w, respectively.

† Note that the author used, in the previous articles referred to, a different scaling factor in his cartesian coordinates. The cartesian coordinates used here are the conventional crystallographic ones defined above.

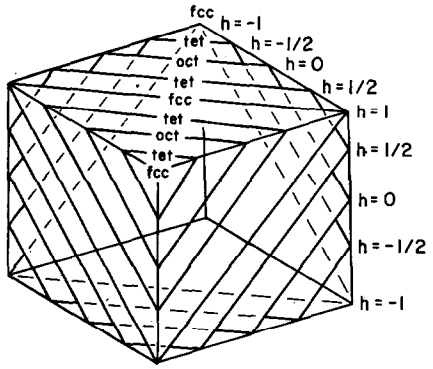

FIG. 6. Sorting out of fcc and interstitial sites by 111 cross sections.

other h equals an even number *plus* $\frac{1}{2}$. We see, therefore, that $h \equiv 2(x + y + z)$ can be used as an index to distinguish the various "interstices" in an fcc array (cf. Fig. 6); if K is any integer:

$h = 2K$ indicates the points of the fcc array.

$h = 2K + \frac{1}{2}$ indicates one set of tetrahedral interstices.

$h = 2K + 1$ indicates octahedral interstices.

$h = 2K + \frac{3}{2}$ indicates the other set of tetrahedral interstices.

For all of these points $v = \sqrt[3]{2h}$; $w = \sqrt[3]{2h}$.

G. The bcc Array

The Frank-Kasper definition yields for the coordination polyhedron of a bcc array the rhombohedral dodecahedron; the obtuse vertices correspond to the nearest neighbors, the acute ones to next nearest neighbors. The fcc and bcc arrays therefore bear an interesting relation to each other. The coordination polyhedron of the bcc array is just the Dirichlet domain of the fcc array. This relationship is the basis of systematically linking fcc and bcc structures. The bcc array is thus characterized by the equations $v = \sqrt[3]{2h}$, $w = \sqrt[3]{2h}$, where h may equal *any* integral multiple of $\frac{1}{2}$.

The Dirichlet domain of the bcc array is *not* the dual of its coordination polyhedron; the construction of Fig. 7 shows in detail how this domain is found. The faces of the cubic unit cell bisect the lines joining next-nearest neighbors, and this cube truncates the faces of an octahedron that bisect the lines joining nearest neighbors. The result is a truncated octahedron whose edges are all of equal length; there are 36 such edges. Since the rhombododecadron was shown to have 24 edges, these two polyhedra cannot possibly be each other's duals.

According to our general definition the interstices of the bcc array are the vertices of the truncated octahedron. Because of the relative proximity of these vertices, complete occupancy of all interstitial sites is rare. One-half occupancy of the bcc array is quite common; the V.E.P. is satisfied if pairs of vertices in each cube face are occupied such that the lines joining the pairs in adjacent faces are mutually perpendicular. The resulting array is shown in Fig. 8; to illustrate the way in which two different conceptual models can be constructed to represent the same physical situation, we show this array in two different "gestalten."

The body-centered array with half of its interstices occupied is exemplified by the Cr_3O structure, better known as the β-W structure (the so-called β-W structure is actually thought to be a tungsten *oxide*). Here the oxide ions occupy a bcc array, the Cr ions the interstices. It will be observed in Fig. 8 that the environment of the oxide ions at the corners of the unit cells is identical with that of the oxide ions at the centers, but that their orientations are 90° apart. Because of these different orientations, the oxide ions belong to two

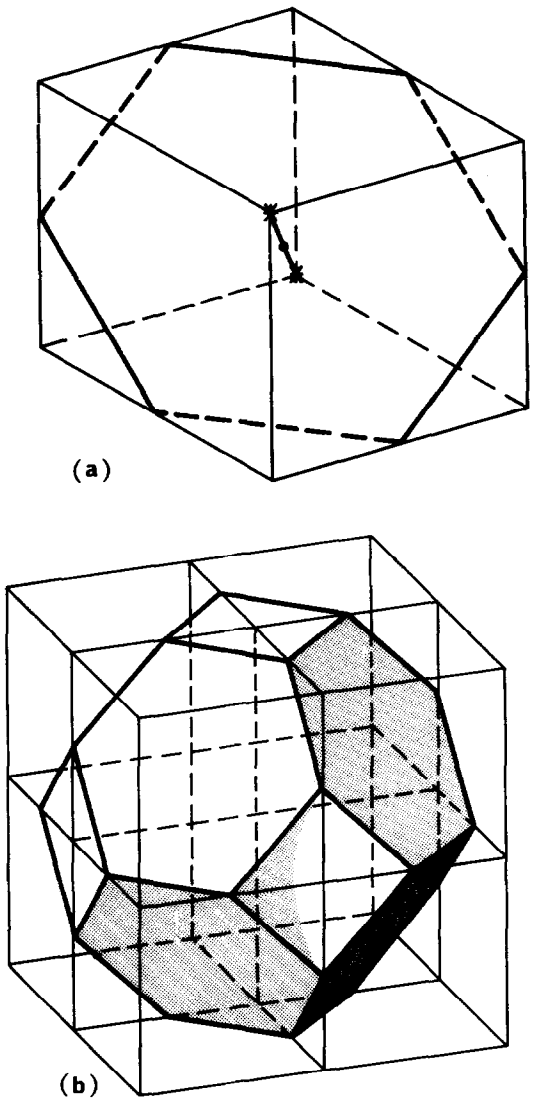

FIG. 7. Construction of the bcc Dirichlet domain. (a) One octant of the bcc unit cell. (b) The entire unit cell with inscribed truncated octahedron.

different primitive lattices rather than to the same bcc lattice. Any classification based on a lattice would place Cr_3O in the *primitive* class, and would obscure the fundamental relation this structure has to the bcc array. We shall, therefore, base our classification not on lattices, but on point complexes, i.e., arrays of points related by translation, reflection or rotation rather than by translation exclusively.

The smallest Cr–O distance in the Cr_3O structure is but 11% greater than the smallest Cr–Cr distance. A structure made up of identical atoms occupying both the bcc array and half of its interstices would not seriously compromise the V.E.P. Therefore, it is not surprising that in β-*W* tungsten, the W and oxide ions are randomly distributed over all these sites. In β-UH_3 the uranium ions actually do occupy the entire β-*W* array. The hydrogen ions are located at ($x = 0$, $y = 0.156 \pm 5$, $z = 0.313$) and the locations related to this by the symmetry operations of group $cPm3n$. It was tempting to search for the general interstices in the array of U ions, and to see whether the hydrogen ions would be anywhere near these interstitial locations. Four noncoplanar U locations were selected, (0 0 0), ($\frac{1}{4}$ 0 $\frac{1}{2}$), ($-\frac{1}{4}$ 0 $\frac{1}{2}$), and (0 $\frac{1}{2}$ $\frac{1}{4}$); the point equidistant from these

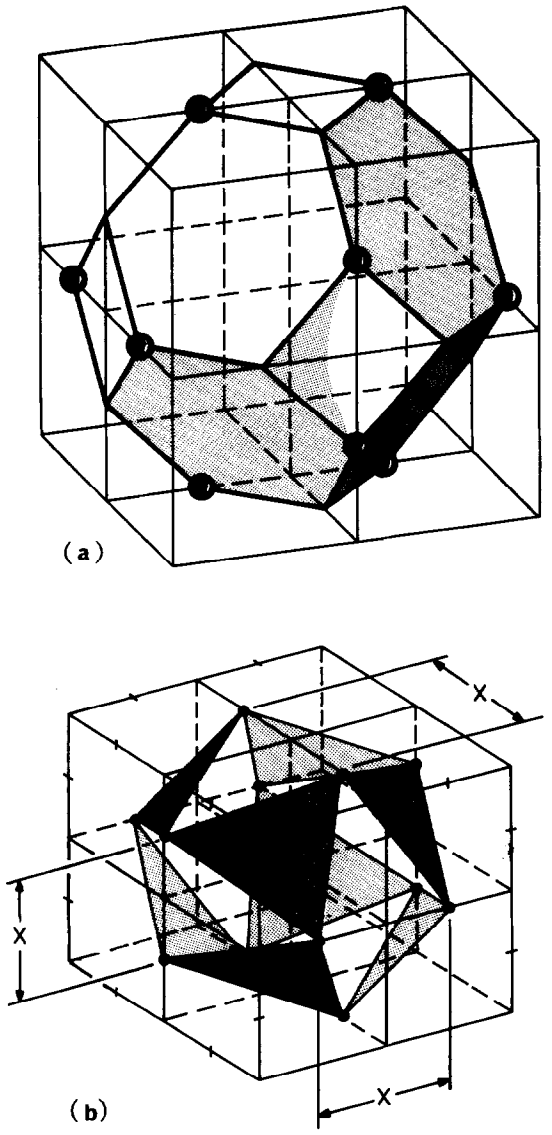

FIG. 8. (a) Relation of the β-W structure to the truncated octahedron of Fig. 7. (b) A different conceptual model for β-W.

four is 0, $\frac{5}{32}$, $\frac{5}{16}$, which in decimal notation becomes (0, 0.156, 0.313), exactly the position of a hydrogen ion! Without a Dirichlet domain as a guide, the significance of the hydrogen locations would have been very difficult to recognize. The procedure in a pattern recognition project is to define first the pattern to search for; the definition of Dirichlet domains and their significance in the definition of interstices constitutes such a first step.

In $AuZn_3$ the Au ions occupy the entire β-W array; the Zn ions have locations ($x = 0$, $y = 0.165 \pm 5$, $z = 0.300 \pm 5$), etc. This structure is now recognized as a slightly distorted form of an ideal interstitial derivative of the β-W structure.

H. The Diamond Array

An important basic array is that formed by the centers of carbon atoms in diamond. This array is not a lattice, as the environments of nearest carbon-atom neighbors are identical but oriented 90° with regard to

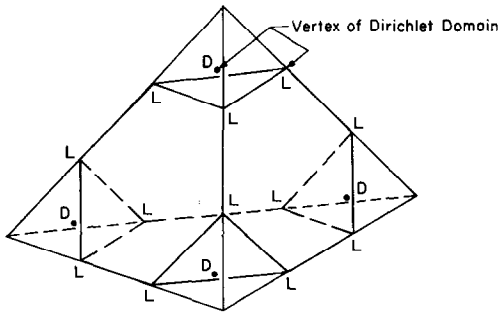

FIG. 9. Dirichlet domain of diamond structure.

each other. The Dirichlet domain of diamond is related to the truncated tetrahedron of Fig. 9, whose edges are all of equal length. By its definition a Dirichlet domain is necessarily a space filler (every point in space must be closer to some point of a regular array than to any other, or else lie on the surface of a Dirichlet domain). The truncated tetrahedron is not a space-filler, but requires a tetrahedron of equal length in one-to-one ratio to fill all of space. Such a tetrahedron can be equally divided between the four surrounding truncated tetrahedra; each portion has as base a face of the tetrahedron, as vertex the center of the tetrahedron; the result is a Dirichlet domain. As shown in Fig. 9, this domain has two types of vertices: twelve, marked *L* are the vertices of the truncated tetrahedron, and four, marked *D*, are the centers of the tetrahedra. Because of their relative proximities, these two types are not simultaneously occupied, but both lead to "interstitial derivatives" of the diamond structure. The *D* vertices by themselves form a second diamond structure, congruent with the first. Together the two diamond structures constitute a bcc structure. The *L* vertices constitute the Cu locations in the Laves phase Cu_2Mg, with the Mg ions occupying the original diamond structure. The Laves phase can thus be interpreted as an interstitial derivative of the diamond structure. We have already seen that in turn these Cu and Mg arrays occur as interstices between fcc oxide ions in spinel. These examples point to a conclusion that there appears to be a rather small number of basic configurations that reoccur in various interpenetrating combinations and permutations in a large variety of different crystals.

I. Point Complexes

A suitable set of basic configurations in terms of which crystals may be expressed, is provided by point complexes. A point complex is an array of symmetrically related points. A lattice is a special kind of point complex whose points are related by translational symmetry. The *multiplicity* of a point complex is defined as the number of points of this complex in a unit cell. Crystal data are implicitly presented in terms of point complexes. Take, for example, the structure of Cu_3S_4V, in a typical format presented by Pearson (*18*):

Cu_3S_4V	$cP\bar{4}3m$	
V: 1*a*	0 0 0	
Cu: 3*c*	$0\,\frac{1}{2}\,\frac{1}{2}$	
S: 4*e*	xxx, $\bar{x}\bar{x}x$	$x = 0.235 \pm 4$

Here, the information $cP\bar{4}3m$ is not of prime importance for our purpose beyond referring to the appropriate page in the International Tables for X-ray crystallography. The important data are 1*a*, 3*c*, 4*e* for these indicate that the respective ions occupy point complexes of multiplicities 1, 3, and 4 whose coordinates are as given in the International Table. The complexes 1*a* and 3*c* have definite, constant coordinates (0 0 0 and $0\,\frac{1}{2}\,\frac{1}{2}$, respectively). These are *invariant* complexes. The complex 4*e* is a *variable* complex, but its coordinates are very near $x = 0.25$; with exactly that value the complex would be *invariant*. We have found by rounding all coordinates off to the nearest multiple of 1/8, it is practically always possible to identify a point complex unequivocally as a distorted form of one of the invariant complexes.

The problem is thus one of identifying and recognizing invariant complexes among crystal data. Unfortunately, the International Tables do not provide their information in a very useful form for this task. The point complexes are arranged according to space group in order of decreasing multiplicity. The complex of highest multiplicity has the most general points, whose coordinates (x, y, z) are all different. In the example under consideration, space group $cP\bar{4}3m$, the most general point complex has multiplicity 24. The next listed complex has points located on mirror planes, so that two of its coordinates are equal, and the 24 points fuse pairwise into a complex of multiplicity 12. Similarly, each space group has a point complex of greatest generality and multiplicity, followed by more specialized locations and lower multiplicity. The invariant complexes appear last and have the lowest multiplicities. The most general complex is uniquely characteristic of a particular space group; the *invariant* complexes recur in many space groups, and are *not* characteristically identified with one particular space group. We shall establish relationships between crystal structures on the basis of the invariant point complexes they have in common. The space group of a crystal is not primarily determined by its invariant complexes, but rather by the peculiar, exceptional ion in a general position; the space group is therefore not a good index for our classification system.

TABLE I

INVARIANT CUBIC POINT COMPLEXES IN ORDER OF INCREASING MULTIPLICITY

Symbol	Coordinates	Brief description and explanation of symbol	Multiplicity
P	0 0 0	primitive	1
P'	$\frac{1}{2}\frac{1}{2}\frac{1}{2}$		
I	0 0 0, $\frac{1}{2}\frac{1}{2}\frac{1}{2}$	bcc array (*i*nner-centered)	2
J	$\frac{1}{2}\frac{1}{2}0$ + cyc.	three-fourth occupied fcc array	3
J'	$\frac{1}{2}0\,0$ + cyc.	("*j*ackstone" configuration)	
F	0 0 0, $\frac{1}{2}\frac{1}{2}0$ + cyc.	fcc array	4
F'	$\frac{1}{2}\frac{1}{2}\frac{1}{2}$, $\frac{1}{2}0\,0$ + cyc.		
F''	$\frac{1}{4}\frac{1}{4}\frac{1}{4}$, $\frac{3}{4}\frac{3}{4}\frac{1}{4}$ + cyc.		
F'''	$\frac{3}{4}\frac{3}{4}\frac{3}{4}$, $\frac{1}{4}\frac{1}{4}\frac{3}{4}$ + cyc.		
${}^{+}Y$	$\frac{1}{8}\frac{1}{8}\frac{1}{8}$, $\frac{7}{8}\frac{5}{8}\frac{3}{8}$ + cyc.	rarely encountered complex in which points occur in a Y-shaped configuration	4
${}^{+}Y'$	$\frac{5}{8}\frac{5}{8}\frac{5}{8}$, $\frac{3}{8}\frac{1}{8}\frac{7}{8}$ + cyc.		
${}^{-}Y$	$\frac{7}{8}\frac{7}{8}\frac{7}{8}$, $\frac{1}{8}\frac{3}{8}\frac{5}{8}$ + cyc.		
${}^{-}Y'$	$\frac{3}{8}\frac{3}{8}\frac{3}{8}$, $\frac{5}{8}\frac{7}{8}\frac{1}{8}$ + cyc.		
W	$\frac{1}{4}0\frac{1}{2}$, $\frac{\bar{1}}{4}0\frac{1}{2}$ + cyc.	one-half of the interstices in the I-complex, as observed in the β-W structure	6
W'	$\frac{1}{2}0\frac{1}{4}$, $\frac{1}{2}0\frac{\bar{1}}{4}$ + cyc.		
D	0 0 0, $\frac{1}{2}\frac{1}{2}0$ + cyc.	diamond structure	8
D'	$\frac{1}{4}\frac{1}{4}\frac{1}{4}$, $\frac{3}{4}\frac{3}{4}\frac{1}{4}$ + cyc.		
	$\frac{1}{2}\frac{1}{2}\frac{1}{2}$, $\frac{1}{2}0\,0$ + cyc.		
	$\frac{3}{4}\frac{3}{4}\frac{3}{4}$, $\frac{3}{4}\frac{1}{4}\frac{1}{4}$ + cyc.		
${}^{+}S$	$\frac{3}{8}0\frac{1}{4}$, $\frac{1}{8}0\frac{3}{4}$ + cyc.	one-quarter occupied W complex	12
	$\frac{7}{8}\frac{1}{2}\frac{3}{4}$, $\frac{5}{8}\frac{1}{2}\frac{1}{4}$ + cyc.		
${}^{-}S$	$\frac{5}{8}0\frac{3}{4}$, $\frac{7}{8}0\frac{1}{4}$ + cyc.		
	$\frac{1}{8}\frac{1}{2}\frac{1}{4}$, $\frac{3}{8}\frac{1}{2}\frac{3}{4}$ + cyc.		
${}^{+}V$	$\frac{1}{8}0\frac{1}{4}$, $\frac{3}{8}0\frac{3}{4}$ + cyc.	another quarter of the W complex (cf. ${}^{+}S$ and ${}^{-}S$)	12
	$\frac{5}{8}\frac{1}{2}\frac{3}{4}$, $\frac{7}{8}\frac{1}{2}\frac{1}{4}$ + cyc.	$W = {}^{+}S + {}^{-}S + {}^{+}V + {}^{-}V$	
${}^{-}V$	$\frac{7}{8}0\frac{3}{4}$, $\frac{5}{8}0\frac{1}{4}$ + cyc.		
	$\frac{3}{8}\frac{1}{2}\frac{1}{4}$, $\frac{1}{8}\frac{1}{2}\frac{3}{4}$ + cyc.		
T	$\frac{1}{8}\frac{1}{8}\frac{1}{8}$, $\frac{3}{8}\frac{3}{8}\frac{1}{8}$, $\frac{3}{8}\frac{7}{8}\frac{5}{8}$ + cyc.	one-half occupied F array: the vertices of the truncated (Laves) tetrahedron	16
T'	$\frac{5}{8}\frac{5}{8}\frac{1}{8}$, $\frac{7}{8}\frac{7}{8}\frac{1}{8}$, $\frac{7}{8}\frac{3}{8}\frac{5}{8}$ + cyc.		
	$\frac{5}{8}\frac{7}{8}\frac{7}{8}$, $\frac{7}{8}\frac{5}{8}\frac{5}{8}$, $\frac{7}{8}\frac{3}{8}\frac{1}{8}$ + cyc.		
	$\frac{1}{8}\frac{1}{8}\frac{5}{8}$, $\frac{3}{8}\frac{3}{8}\frac{5}{8}$, $\frac{3}{8}\frac{7}{8}\frac{1}{8}$ + cyc.		

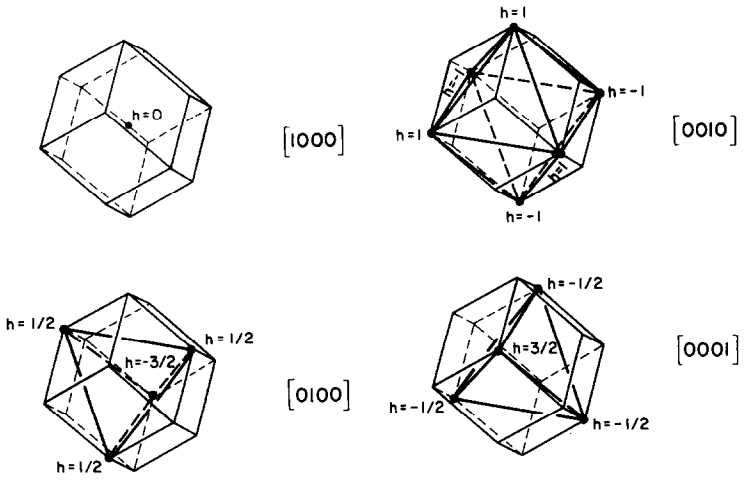

FIG. 10. *F* complexes as distributions over the sites of the *I* complex.

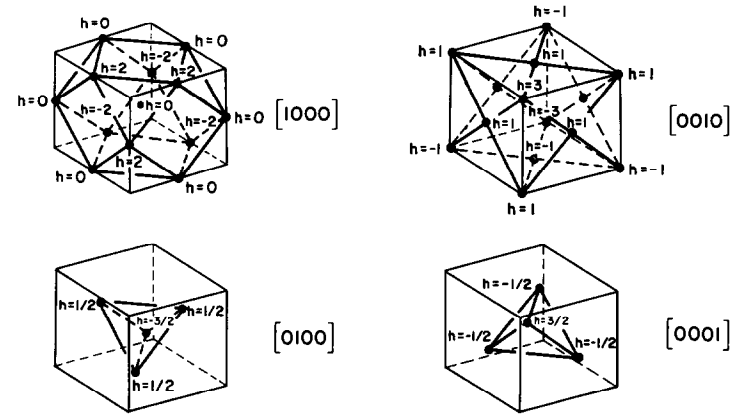

FIG. 11. The *F* complexes related to the cubical unit cell.

The International Tables list all point complexes occurring under every space group. However, these tables do *not* identify the same complex by a unique symbol regardless of the space group under which it is listed. For instance, the same point complex is called 8*c* when listed under space group *cFm*3*m*, but 8*a* under space group *cFm*3*c*. A nomenclature was, therefore, developed by Hermann, Hellner, etc. (*19*, *20*, *21*), in which each point complex was given a unique symbol regardless of its context. Of these, the cubic invariants are listed in Table I, rearranged in order of increasing multiplicity to show that multiplicity rather effectively characterizes an invariant point complex. For our example of Cu_3S_4V, the V ions obviously are located on a *P* complex, Cu is at once identified with the *J* complex, and it is not hard to imagine that the distortion of an *F* complex from $x = \frac{1}{4}$ to $x = 0.235$ would produce just the complex of sulphide ions.

It may appear surprising that a complex of multiplicity 6, the *W* complex, when half-occupied should yield a complex of multiplicity 12, viz., the *S* and *V* complexes. The reason is that symmetrical half-occupancy of the *W* complex necessitates the scaling of the unit cell by a linear factor 2. Such scaling multiplies the multiplicity by 8, and is indicated by a subscript 2; the complex *W*, multiplicity 6, is transformed into W_2, multiplicity 48, which is then subdivided into the four complexes of multiplicity 12 each. The geometry of these subdivisions will be discussed presently.

Different positions of a complex relative to the unit cell are distinguished by primes. It should be emphasized that the complexes so distinguished are congruent, and not essentially different from each other, although they often appear different when inscribed in a unit cell (Figs. 10 and 11).

J. The Algebra and Geometry of Cubic Invariant Complexes

From crystallographic data we can glean the following information: (1) the invariant point complexes can be identified, their multiplicity being the principal clue; (2) the cartesian coordinates of the variable complexes can be rounded off to the nearest multiple of $\frac{1}{8}$, so that these complexes can become identified with invariant complexes of the same multiplicities. As a result, the crystal is described as a combination of interpenetrating invariant complexes; crystals that have invariant complexes in common are said to be related in the sense of our system of organization. To be useful as a conceptual model, this description needs some geometrical interpretation.

It will be convenient to start with an I complex; Table I informs us that it corresponds to a bcc array. In Section G we found that the bcc array has a rhombododecahedron as coordination polyhedron, and in Section F we discovered that this same polyhedron is also the Dirichlet domain of the fcc array (Fig. 5b). We can conclude, therefore, that the I complex is made up of an F complex *plus* all its interstices. We also discovered in Section F that each of these sets of interstices constitutes an array congruent to the F complex. A simple coordinate transformation identifies the fcc array with $F(h = 2K)$ the octahedral interstices with $F'(h = 2K + 1)$, one set of tetrahedral interstices with $F''(h = 2K + \frac{1}{2})$, and the other set of tetrahedral interstices with $F'''(h = 2K + \frac{3}{2})$. Therefore, $I = F + F' + F'' + F'''$.

The author (*1, 3, 4, 6*) has developed a very simple matrix notation for these various arrays, in which the columns correspond to different values of K and the rows to different combinations of values of v and w. (N.B. Since publication of these four articles it was decided to interchange rows and columns.) Since we have so far been concerned only with four possible values of h: $2K$, $2K + \frac{1}{2}$, $2K + 1$, and $2K + \frac{3}{2}$ (the patterns repeat after two units in h), we need but four columns. The h planes have so far been either closely packed or not occupied at all, so that a single row is needed; an entry 1 in the matrix indicates complete occupancy, a 0 an empty h plane. In terms of this notation these so-called distribution matrixes become

$$F = [1\ 0\ 0\ 0], \quad F'' = [0\ 1\ 0\ 0], \quad F' = [0\ 0\ 1\ 0], \quad F''' = [0\ 0\ 0\ 1].$$

Figure 10 shows the geometric arrangement of these complexes as distribution over the center and vertices of the rhombododecahedron, and Fig. 11 shows them related to the cubic unit cell.

Furthermore, the diamond structure can be interpreted as an fcc array with one of the set of tetrahedral interstices occupied, so that

$$D = [1\ 1\ 0\ 0] = F + F'', \quad D'[0\ 0\ 1\ 1] = F' + F''' \text{ (Fig. 12).}$$

Other possible diamond point complexes not explicitly mentioned by Hellner would be [1 0 0 1] and [0 1 1 0].

The P complex could be considered as an fcc array plus its octahedral interstices:

$$P_2 = [1\ 0\ 1\ 0] = F + F'; \quad P_2' = [0\ 1\ 0\ 1] = F'' + F'''.$$

We know that we must use the subscript 2 in these cases, because a single column corresponds to an F array, i.e., four points per unit cell. Therefore, the two interpenetrating F arrays produce eight points per unit cell.

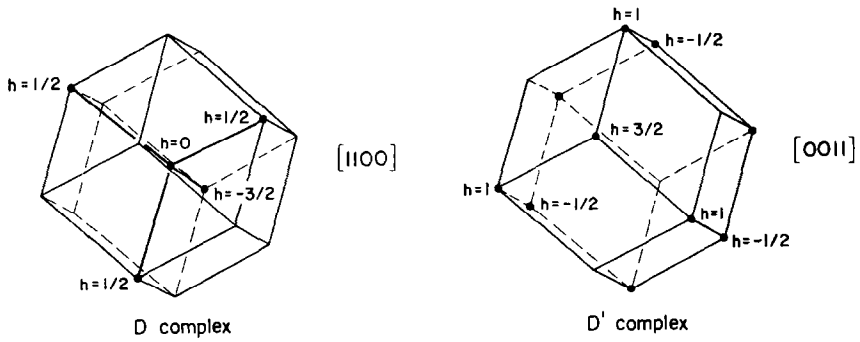

FIG. 12. The D complex.

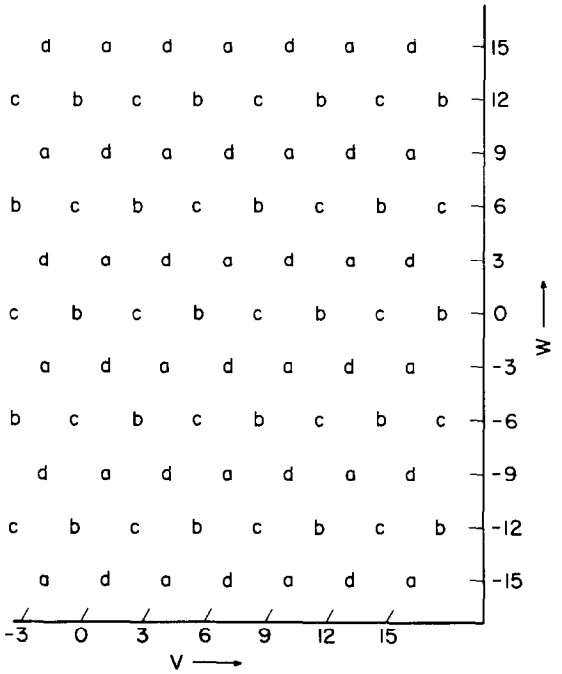

FIG. 13. Subdivision of hexagonal net into four equivalent subnets.

In the case of the D complex the resulting cell is the smallest possible, but for the P complex the resulting cell consists of eight identical octants in identical orientation, which therefore contains eight of the smallest possible P cells.

Finally

$$I_2 = [1\ 1\ 1\ 1] = F + F' + F'' + F'''$$

hence,

$$D + D' = [1\ 1\ 0\ 0] + [0\ 0\ 1\ 1] = [1\ 1\ 1\ 1] = I_2.$$

It is also possible to indicate in the distribution matrix occupancy by a particular element. For example, rocksalt becomes simply [Cl 0 Na 0], diamond [C C 0 0], and sphalerite [S Zn 0 0].

The J complex is a three-quarter occupied F complex. Here, the h planes are themselves partially occupied. Figure 13 shows the sites in such a plane, symmetrically subdivided into four mutually congruent subsets [cf. Loeb (*1*)] labeled a, b, c, and d. These four sets of sites are characterized by the parities of their v and w coordinates: a has odd v and w, b has odd v and even w, c has even v and w, and d has even v and odd w. Partial occupancy of an h plane can be indicated by a combination of zeros and ones in the appropriate column of the distribution matrix:

$$\text{the } a \text{ sites are denoted by } \begin{bmatrix}1\\0\\0\\0\end{bmatrix}, b \text{ by } \begin{bmatrix}0\\1\\0\\0\end{bmatrix}, c \text{ by } \begin{bmatrix}0\\0\\1\\0\end{bmatrix}, \text{ and } d \text{ by } \begin{bmatrix}0\\0\\0\\1\end{bmatrix}.$$

The J complexes are then

$$J = \begin{bmatrix}1&0&0&0\\1&0&0&0\\0&0&0&0\\1&0&0&0\end{bmatrix}, \qquad J' = \begin{bmatrix}0&0&1&0\\0&0&1&0\\0&0&0&0\\0&0&1&0\end{bmatrix}.$$

They are illustrated in Fig. 14.

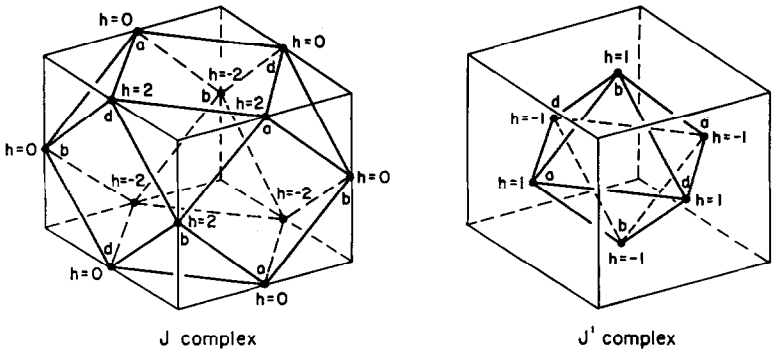

FIG. 14. The J complex.

It is interesting to see what the one-quarter of the F complex that is left unoccupied by J looks like. Its distribution matrix, which we shall for the time being call X, is

$$X = \begin{bmatrix} 0 & 0 & 0 & 0 \\ 0 & 0 & 0 & 0 \\ 1 & 0 & 0 & 0 \\ 0 & 0 & 0 & 0 \end{bmatrix}$$

This is a very "dilute" structure of multiplicity 1. Table I would lead us to suspect that it might be a P array. We know that $P_2 = [1\ 0\ 1\ 0]$. If we "dilute" P_2 by a linear factor of 2, we occupy, in fact, only one-quarter of each occupied h plane, and we separate the h planes by twice the original distance. Comparison of the matrices of X and P_2 shows that, indeed, $X = P$.

$$\therefore J + P = \begin{bmatrix} 1 & 0 & 0 & 0 \\ 1 & 0 & 0 & 0 \\ 1 & 0 & 0 & 0 \\ 1 & 0 & 0 & 0 \end{bmatrix} = [1\ 0\ 0\ 0] = F.$$

The same dilution procedure (replacing a column 1 by a column of a single 1 and three zeros and inserting a column of zeros between all adjacent columns) gives the distribution matrix for I from $I_2 = [1\ 1\ 1\ 1]$:

$$I = \begin{bmatrix} 0 & 0 & 0 & 0 \\ 0 & 0 & 0 & 0 \\ 1 & 0 & 1 & 0 \\ 0 & 0 & 0 & 0 \end{bmatrix}$$

The T complex is also conveniently expressed in terms of a distribution matrix, but here the repeat distance in h is four units instead of two:

$$T = \begin{bmatrix} 0 & 0 & 0 & 1 & 0 & 0 & 0 & 0 \\ 0 & 0 & 0 & 0 & 0 & 0 & 0 & 1 \\ 0 & 0 & 0 & 0 & 0 & 0 & 0 & 1 \\ 0 & 0 & 0 & 0 & 0 & 0 & 0 & 1 \end{bmatrix}; \quad T' = \begin{bmatrix} 0 & 0 & 0 & 0 & 0 & 0 & 0 & 1 \\ 0 & 0 & 0 & 1 & 0 & 0 & 0 & 0 \\ 0 & 0 & 0 & 1 & 0 & 0 & 0 & 0 \\ 0 & 0 & 0 & 1 & 0 & 0 & 0 & 0 \end{bmatrix}$$

$$\therefore T + T' = [1\ 0\ 0\ 0\ 1\ 0\ 0\ 0] = [1\ 0\ 0\ 0] = F.$$

It should be emphasized that cyclic permutations of either the rows or the columns simply correspond to a change in origin. The particular expressions given above result from the historical accidents of choice of origins made by Hellner and by this author.

Hellner uses an asterisk for composites of mutually congruent point complexes: $J^* \equiv J + J'$.

TABLE II

SUMMARY OF MATRIX NOTATION FOR POINT COMPLEXES

$$P = \begin{bmatrix} 0 & 0 & 0 & 0 \\ 0 & 0 & 0 & 0 \\ 1 & 0 & 0 & 0 \\ 0 & 0 & 0 & 0 \end{bmatrix}; \quad P_2 = [1 \quad 0 \quad 1 \quad 0]; \quad P_2' = [0 \quad 1 \quad 0 \quad 1]$$

$$I = \begin{bmatrix} 0 & 0 & 0 & 0 \\ 0 & 0 & 0 & 0 \\ 1 & 0 & 1 & 0 \\ 0 & 0 & 0 & 0 \end{bmatrix}; \quad I_2 = [1 \quad 1 \quad 1 \quad 1]$$

$$J = \begin{bmatrix} 1 & 0 & 0 & 0 \\ 1 & 0 & 0 & 0 \\ 0 & 0 & 0 & 0 \\ 1 & 0 & 0 & 0 \end{bmatrix}; \quad J' = \begin{bmatrix} 0 & 0 & 1 & 0 \\ 0 & 0 & 1 & 0 \\ 0 & 0 & 0 & 0 \\ 0 & 0 & 1 & 0 \end{bmatrix}; \quad J^* = \begin{bmatrix} 1 & 0 & 1 & 0 \\ 1 & 0 & 1 & 0 \\ 0 & 0 & 0 & 0 \\ 1 & 0 & 1 & 0 \end{bmatrix}$$

$F = [1 \quad 0 \quad 0 \quad 0]; \quad F' = [0 \quad 0 \quad 1 \quad 0]; \quad F'' = [0 \quad 1 \quad 0 \quad 0]; \quad F''' = [0 \quad 0 \quad 0 \quad 1]$

$D = [1 \quad 1 \quad 0 \quad 0]; \quad D' = [0 \quad 0 \quad 1 \quad 1]$

$$T = \begin{bmatrix} 0 & 0 & 0 & 1 & 0 & 0 & 0 & 0 \\ 0 & 0 & 0 & 0 & 0 & 0 & 0 & 1 \\ 0 & 0 & 0 & 0 & 0 & 0 & 0 & 1 \\ 0 & 0 & 0 & 0 & 0 & 0 & 0 & 1 \end{bmatrix}; \quad T' = \begin{bmatrix} 0 & 0 & 0 & 0 & 0 & 0 & 0 & 1 \\ 0 & 0 & 0 & 1 & 0 & 0 & 0 & 0 \\ 0 & 0 & 0 & 1 & 0 & 0 & 0 & 0 \\ 0 & 0 & 0 & 1 & 0 & 0 & 0 & 0 \end{bmatrix}$$

TABLE III

INTERRELATIONS BETWEEN INVARIANT CUBIC POINT COMPLEXES

	P	I	J	F	D	T
P	$P_2 + P_2' = I_2$ $P + P' = I$	$P_2 + P_2' = I_2$ $P + P' = I$ $I + J^* = P_2$	$P + J = F$ $I + J^* = P_2$	$P + J = F$ $F + F' = P_2$		
I			$I + J^* = P_2$	$F + F' + F'' + F''' = I_2$	$D + D' = I_2$	
J			$J + J' = J^*$	$P + J = F$		
F				The F's are interstitially related $F + F' = P_2$, etc. $F + F'' = D$, etc. $F + F' + F'' + F''' = I_2$	$F + F'' = D$ $F' + F''' = D'$	$T + T' = F$
D					D' and D are interstitially related	T is interstitial to D
T						$T + T' = F$

These invariant complexes completely describe what can be equally well regarded as substitutional derivatives of the I_2 complex, or interstitial derivatives of the F complex. Their matrix representations and interrelationships are summarized in Tables II and III. (The relations expressed in Table III can be easily proven using the matrices of Table II.)

The interstitial derivatives of the I complex are the W, S, and V complexes, all of which represent distributions over the Dirichlet domain of an I complex. W and W' represent half occupancies of these interstices, as shown in Fig. 8; the entire complex of vertices is called W^*: $W^* = W + W'$. In Fig. 8b, the distance x may be varied from 0 to 1. The shaded triangles should be imagined as being hinged to each other at their corners, being free to rotate around the body diagonal perpendicular to themselves, meanwhile sliding along this diagonal but remaining parallel to themselves. The black dots then represent a J' complex when $x = 0$ (the triangles then enclose a regular octahedron), and a J complex when $x = 1$ (the black dots are vertices of a cuboctahedron), as shown in Fig. 14. When $x = \frac{1}{2}(\sqrt{5} - 1) \doteq 0.62$, the dots represent the vertices of a regular icosahedron, and when $x = \frac{1}{2}$, the dots represent a W (or W') complex.

One-quarter occupancy of the Dirichlet domain vertices produces the S^* and V^* complexes. Of every pair of points in a face of the cubic cell one point belongs to S^*, the other to V^* (Fig. 15). Note that two of the eight triangles have three vertices all marked V, but that there are no triangles having all vertices labeled S. The S^* and V^* complexes are therefore not equivalent: it is not possible to subdivide the W complex into two equivalent halves. Furthermore, the opposite faces of the cube of Fig. 15 are *not* related by translational symmetry, for a translation of one face into an opposite one turns an S site into V, and vice versa. Therefore, this cube can not be a unit cell, but represents one octant of a unit cell. The W complex has multiplicity 6, hence W_2 has multiplicity 48, and S^* and V^*, comprising half of the W_2 sites, each having multiplicity 24. Further subdivision of S^* and V^* into ${}^+S$, ${}^-S$, ${}^+V$, and ${}^-V$ is accomplished by noting that the center of the cube of Fig. 15 lies on the middle of lines joining pairs of S's and of V's. The two points on opposite ends of such lines are arbitrarily called + and −. The result is the set of four complexes each comprising a quarter of the W complex and having multiplicity 12. Thus we complete the algebraic and geometrical interpretation of Hellner's invariant cubic point complexes.

K. Models

The matrix notation described in the previous section is conveniently implemented by special models, consisting of space-filling modules that may contain a sphere at their center or may be empty. These can be stacked together in various permutations and combinations without special connectors. Some of these,

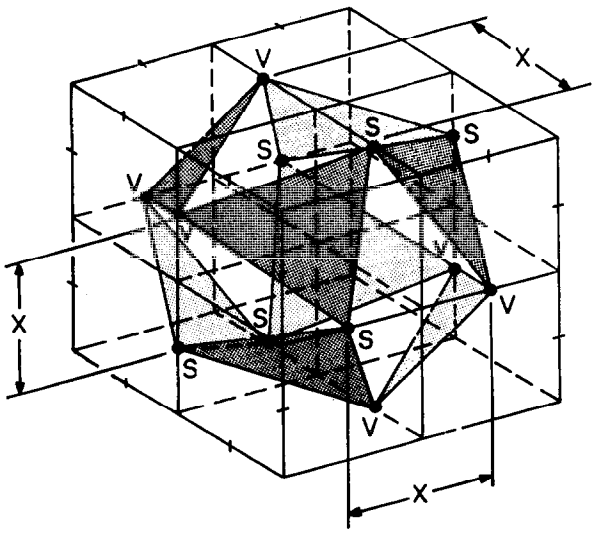

FIG. 15. Subdivision of the W complex into V^* and S^* complexes.

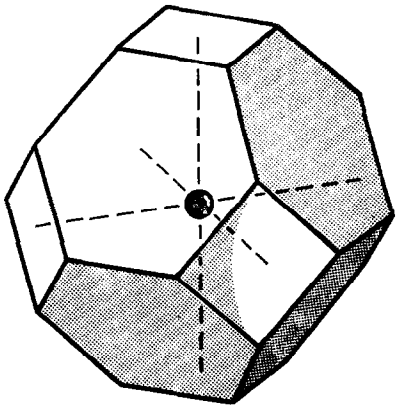

FIG. 16. Domuledron crystal building block.

Moduledra crystal building blocks,† have been described previously (*22*). They consist of filled or empty tetrahedra and octahedra. *Centers* of close-packed spheres are represented by the vertices of the Moduledra; each moduledron is either empty or contains a sphere, depending on whether the interstice it represents is empty or occupied. Both cubic and hexagonal structures may be represented by these modules, but either some or all of the ions must be close-packed.

Many alloys do not contain closely packed ions. For example, in $AuCu_3$ the combined metal ions form a close-packed array, but Au forms a P complex, and Cu a J complex ($P + J = F$), and the corners of the moduledra cannot be marked to distinguish Au from Cu ions. Since the centers of either set of tetrahedra and of the octahedra individually constitute an F array, it is possible to represent $AuCu_3$ with tetrahedra or octahedra containing spheres of two different colors. The vertices of the moduledra would then not represent anything. Similarly, a model for spinel could represent Cu_2Mg if the vertices of the moduledra are ignored. However, where fractions of all of the four F complexes (F, F', F'', and F''') are simultaneously occupied, moduledra cannot be used. A different module was therefore designed whose shape is that of the Dirichlet domain of the I complex (Fig. 16), and which is, therefore, called Domuledron. At the center of the Domuledron there may or may not be a colored sphere. When Domuledra containing identical spheres are stacked together to fill space, the spheres constitute an I complex. The Domuledra may be stacked with their square faces horizontal, in which case two cartesian axes are horizontal, the third vertical, or with hexagonal faces horizontal, in which case the h axis will be vertical. In the latter mode, the centers of the modules constitute, in any horizontal plane, the sites of Fig. 13. Occupancy of these sites is indicated by the distribution matrix of a given structure, and modeled by Domuledra of different (un)occupancies.

To guide in translating a distribution matrix into a model, a decoding device called the Crystograph‡ has been constructed (Fig. 17). When the distribution matrix is entered on the switchbox, one value of h at a time, the corresponding plane is displaced on the screen in the correct position. Both the Moduledra and Domuledra are commensurate with the screen of the Crystograph, so that the screen in horizontal position can function as a floor plan for the model, which is constructed on top of it, layer by layer, from Moduledra or Domuledra.

L. Classification and Representation of Actual Structures

We have seen how crystal data can be expressed as superpositions of idealized interpenetrating arrays, the cubic invariant point complexes, how in the substitutional derivatives of the bcc lattice (interstitial derivatives of the fcc lattice) they can be expressed as distribution matrices, and how these matrices may in turn be translated into models made up of very few basic modules. We shall now consider the field of about 2,000 cubic crystal structures reported by W. B. Pearson (*18*) and classify them according to how they are interrelated. Pearson's structures belong to 85 different structure types, and for eleven of these experimental

† Trademark Registered.
‡ U.S. Patent No. 3,368,290.

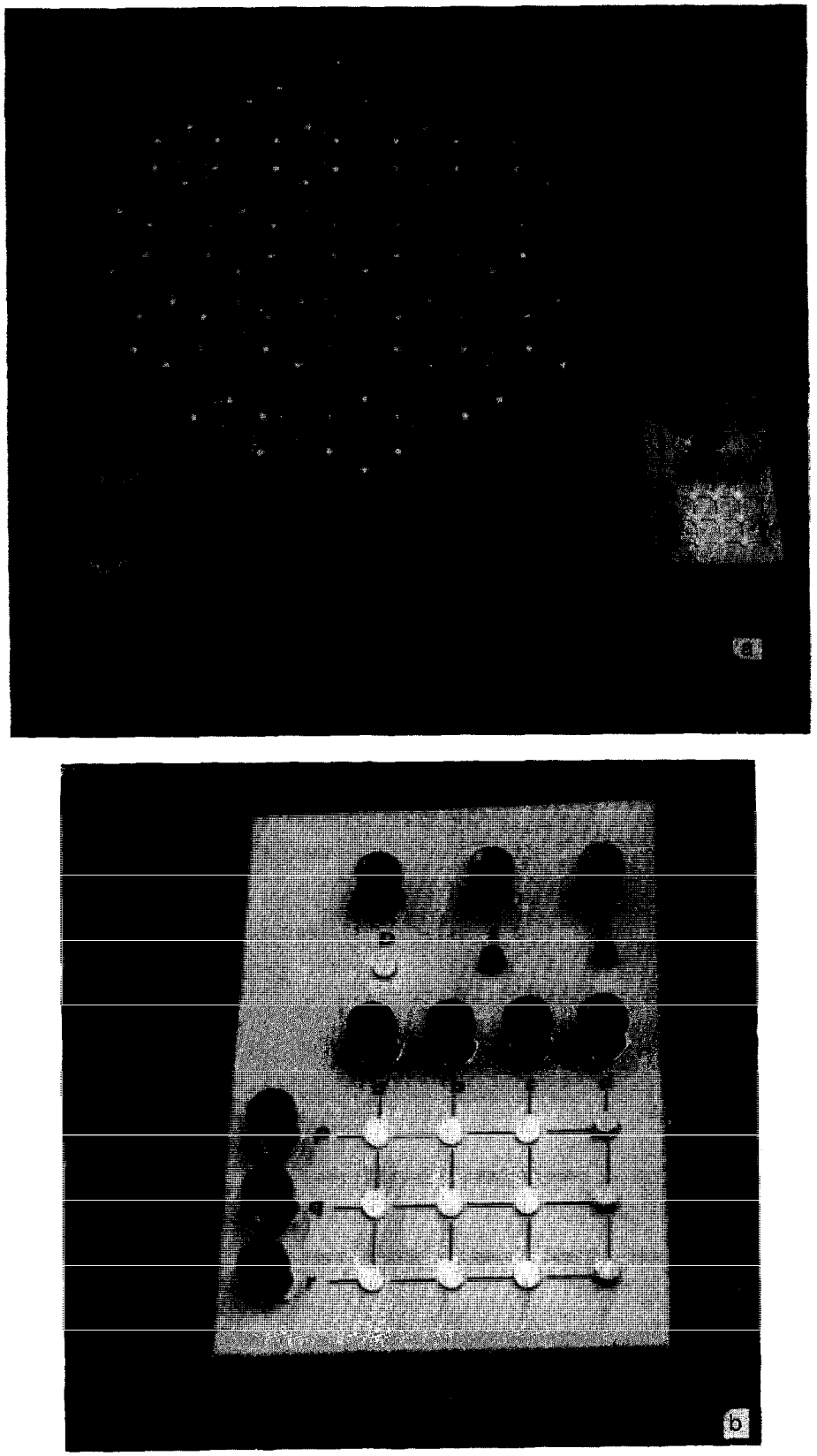

FIG. 17. The Crystograph. (a) Display panel. (b) Console.

data are incomplete, so that no classification is possible. In Table IV these structure types are listed in decreasing order of "population," where population is interpreted as the number of different isomorphs reported for a given structure type. It is notable that 59 structures are bcc, while only 32 are fcc. However, 147 structures belong to the $AuCu_3$ type, a substitutional derivative of the *F* complex.

We have classified the 74 structure types into five groups:

1. Substitutional derivatives of the *I* complex (55 structure types, representing about 1,700 structures).
2. Special nets having equally spaced nodes (six structure types, representing about 100 structures).
3. Interstitial derivatives of the *I* complex (six structure types, representing about 150 structures).
4. The Mn structures (represent about 48 structures).
5. Miscellaneous structure types that are idiosyncratic, bearing no apparent relationship either to each other or to other structure types (8 structure types, representing about 30 structures).

There is some overlap between these groups because some structures could belong to more than one group, depending on the way of looking at it. Such overlap is very infrequent. A survey of the structures now follows:

TABLE IV

STRUCTURE TYPES IN DECREASING ORDER OF POPULATION

Structure type	Number of isomorphs	Structure type	Number of isomorphs	Structure type	Number of isomorphs
NaCl (rocksalt)	258	As_3Co	12	$Be_{17}Ru_3$	2
CsCl	233	Co_9S_8	11	γ-Mo_3N_2	1
Cu_2Mg	196	C_3Pu_2	11	Li_7MnN_4	1
$AuCu_3$	147	UB_{12}	10	β-Ni_3S_2	1*
CaF_2	101	$BaHg_{11}$	10	Cu_5FeS_4	1
β-$W(Cr_3O)$	67	Cu_3S_4V	9	Cu_2Se	1
$AlCu_2Mn$	63	Ge_7Ir_3	8	Ca_7Ge	1
CFe_3W_3 and $NiTi_2$	63	$AuBe_5$	8	$Ca_{33}Ge$	1
Ce_2S_3 and P_4Th_3	61	S_4Tl_3V	6	S_4Zr_3	1
W(bcc)	59	GeK	6	Al_2S_3	1
ZnS (sphalerite)	58	$Cu_{15}Si_4$	6	Cu_3S_4Sb	1
FeS_2	52	$Zn_{22}Zr$ (E-$Al_{18}Cr_2Mg_3$)	5	α-$Al_{13}Cr_4Si_4$	1
Al_2MgO_4 (spinel)	46	$Al_{12}W$	5	α-In_2Te_3	1
$CaTiO_3$ and ReO_3	46	Cu_5Zn_8	5	ζ-$Mg_{\sim 6}Pd$	1*
α-Mn	36	CuSB(L.T.)	5*	Cd_3Cu_4	1*
$NaZn_{13}$	36	$GeLi_5N_3$ and $AlLi_3N_2$	5	Cd_2Na	1*
BiF_3	36	α-Po	4	β-Al_3Mg_2	1*
Cu(fcc)	32	CFe_4	4	CoU	1
β-Mn_2O_3	31	Al_4Cu_9	4	Si III	1
$Cu_{16}Mg_6Si_7$	29	$Pd_{17}Se_{15}$	4	Ag_8Ca_3	1*
FeSi	25	C (diamond)	4	Ag_3AuTe_2	1
NiSSb	24	$Li_{22}Pb_5$	4	Sb_2Tl_7	1
AgAsMg	24	Hg_4Pt	4	$Cu_{12}S_{13}Sb_4$	1
CaB_6	23	Cu_2O	3	β-$CuFeS_2$	1
C_6Cr_{23}	16	$(Al, Zn)_{49}Mg_{32}$	3	Q-$Al_7Cu_3Mg_6$	1*
$Mn_{23}Th_6$	14	$AuZn_3$ and β-UH_3	2	$AsCu_3S_4$	1*
Cd_6Ce	14*	Mg_2Zn_{11}	2	Bi_4Rh	1
NaTl	13	Cu_4MgSn	2*		
β-Mn and Al_2CMo_3	12	Fe_3Zn_{10}	2		

* Insufficient experimental data for the purpose of classification.

1. Substitutional Derivatives of the *I* complex

These are the 55 structure types that are considered as distributions over the bcc lattice, and for which models can be built with Domuledra or Moduledra models. Because these represent about three-quarters of all cubic structure types, a subclassification is made: first, distributions over all the points of the *F* complex (distribution matrix [1 0 0 0]); next, distributions over all the points of the *D*-lattice complex (distribution matrix [1 1 0 0]); then, distributions over all the points of the *P* complex (distribution matrix [1 0 1 0]) and over an array with distribution matrix [1 1 0 1], followed by distributions over all the points of the complete *I* complex (distribution matrix [1 1 1 1]). Finally, there are partial occupancies of these complexes and some special cases.

a. *F* Complex. The 32 structures whose atoms form a fcc lattice are represented by structure-type Cu whose distribution matrix is:

[Cu 0 0 0].

There are 147 binary alloys whose atoms distribute themselves symmetrically over an *F* complex. They are represented by structure type $AuCu_3$:

$$\begin{bmatrix} Au & 0 & 0 & 0 \\ Cu & 0 & 0 & 0 \\ Cu & 0 & 0 & 0 \\ Cu & 0 & 0 & 0 \end{bmatrix}.$$

A unique structure is Ca_7Ge, in which one-eighth of the *F* complex is occupied by Ge, the remainder by Ca:

$$\begin{bmatrix} Ge & 0 & 0 & 0 & Ca & 0 & 0 & 0 \\ Ca & 0 & 0 & 0 & Ca & 0 & 0 & 0 \\ Ca & 0 & 0 & 0 & Ca & 0 & 0 & 0 \\ Ca & 0 & 0 & 0 & Ca & 0 & 0 & 0 \end{bmatrix}.$$

b. *D* Complex. The following are structures in which the atoms distribute themselves over all locations of the *D* complex.

Diamond: [C C 0 0].

Anions and cations separately occupy *F* complexes; their juxtaposition is such that jointly they occupy the *D* complex.

Sphalerite: [S Zn 0 0].

Cu_3S_4V: The sulphide ions form a slightly distorted fcc array ($x = y = z = 0.235 \pm 4$, ideally 0.250). Cu and V occupy the tetrahedral interstices between the sulphide ions, with the tetrahedra around V slightly contracted.

$$\begin{bmatrix} S & V & 0 & 0 \\ S & Cu & 0 & 0 \\ S & Cu & 0 & 0 \\ S & Cu & 0 & 0 \end{bmatrix}.$$

α-In_2Te_3: The unit cell has 180 atoms; 108 Te form $3 \times 3 \times 3$ fcc cells of four atoms each; 72 In atoms occupy one-third of the tetrahedral interstices, i.e., two-thirds of the Zn sites in a sphalerite structure:

[Te $In_{2/3}$ 0 0].

The occupancy of two-thirds of the In sites is very special, since graphite layer-like patterns are formed in all planes perpendicular to cube diagonals. The occupied sites have the following coordinates:

$$\overset{6}{h} = \tfrac{1}{2}\colon \overset{9}{(v - w)} = 3 \text{ or } 6,$$

$$\overset{6}{h} = \tfrac{5}{2}\colon \overset{9}{(v, w)} = 03, 30, 33, 36, 63, \text{ or } 66,$$

$$\overset{6}{h} = \tfrac{9}{2}\colon \overset{9}{(v, w)} = 06, 60, 66, 63, 36, \text{ or } 33.$$

c. *P* Complex. There are only four structures whose atoms form a primitive cubic lattice. They are represented by the structure type α – Po whose distribution pattern is

[Po 0 Po 0].

The *P* complex is made up of two interpenetrating *F* complexes. When one of these is occupied by Cl and the other by Na, the NaCl structure type, representing 258 structures, results:

[Cl 0 Na 0].

Closely related to the NaCl structure is Zr_3S_4(?), a defect structure in which vacancies are randomly distributed over half the Na sites. In the distribution matrix the combination of Zr and vacancies is indicated by Zr′:

$$\begin{bmatrix} S & 0 & Zr & 0 & S & 0 & Zr' & 0 \\ S & 0 & Zr' & 0 & S & 0 & Zr & 0 \\ S & 0 & Zr' & 0 & S & 0 & Zr & 0 \\ S & 0 & Zr' & 0 & S & 0 & Zr & 0 \end{bmatrix}.$$

A second defect structure of the NaCl type is γ-Mo_3N_2, in which three-fourths of the Na type sites are randomly occupied by *N* and vacancies. Its distribution matrix is approximately

$$\begin{bmatrix} Mo & 0 \sim \frac{1}{3}N & 0 \\ Mo & 0 \sim \frac{1}{3}N & 0 \\ Mo & 0 \sim \frac{1}{3}N & 0 \\ Mo & 0 \quad N & 0 \end{bmatrix}.$$

Other, special derivatives of the NaCl structure will be discussed in more appropriate locations.

d. The Array [1 1 0 1] and Its Derivatives. No substance is known whose distribution matrix is [1 1 0 1]. However, there are many derivatives of this hypothetical structure. Principal among them is the structure type CaF_2, representing 101 structures. Its distribution matrix is

[Ca F 0 F].

Also important is AgAsMg, which represents 24 structures:

[As Mg 0 Ag].

Related is also Cu_2Se (H.T.), with the probable distribution matrix:

[Cu Cu 0 Se].

Here, one-eighth of the Cu's randomly deviate from the ideal array. Experimental data are inconclusive.

Also distributed over the [1 1 0 1] array are the atoms of Li_7MnN_4. Here Li and Mn are in an ordered distribution over fluoride sites in a CaF_2 type structure. There is a slight distortion of one-fourth of the N atoms from an ideal fcc array: $x = 0.115$, ideally 0.125. The distribution matrix is

$$[N(Li_{7/8}, Mn_{1/8})\ 0\ (Li_{7/8}, Mn_{1/8})].$$

Also derived from CaF_2 is Cu_5FeS_4(H.T.), where 5 Cu and Fe appear to be randomly distributed over the *F* site

$$[S(Cu_{5/8}Fe_{1/8})\ 0\ (Cu_{5/8}Fe_{1/8})].$$

In β-$CuFeS_2$ the fluoride sites are occupied in an ordered fashion by Cu and Fe.

$$[S(Cu_{1/4}Fe_{1/4})\ 0\ (Cu_{1/4}Fe_{1/4})].$$

In $AlLi_3N_2$ we encounter the *Y*** complex, which constitutes one-fourth of a *P* complex. The subdivision is not the usual one according to the parities of coordinates *v* and *w*, but a special one in which the sites

occupied by Al form Y shaped arrays in h planes, whence the name of the complex. The coordinates for the Y^{**} complex obey the conditions:

$$\overset{4}{h} = \tfrac{1}{2}, \tfrac{5}{2}: (v - 2h), (w - 2h) \overset{12}{=} 33, 03, 60, 36,$$

$$\overset{4}{h} = -(\tfrac{1}{2}, \tfrac{5}{2}): (v - 2h), (w - 2h) \overset{12}{=} -(33, 03, 60, 36).$$

The Li atoms occupy the remaining three-quarters of the fluoride sites. There is a distortion for the Li positions:

$$x = 0.160, \text{ ideally } 0.125,$$

$$y = 0.382, \text{ ideally } 0.375,$$

$$z = 0.110, \text{ ideally } 0.125.$$

The N ions together form an fcc array. Two-thirds of these N ions are displaced from ideal locations. For these the distortions are: N(2)24d: $x = 0.205$, ideally 0.25.

A further derivative is β-Mn_2O_3, which has a defect CaF_2 structure:

$$[MnOx_{3/4} - Ox_{3/4}].$$

The oxide ions occupy three-fourths of the F sites in such a way that the unoccupied fluoride sites form a Y^{**} complex. The oxide array is somewhat distorted:

$$x = 0.385, \text{ ideally } 0.375,$$

$$y = 0.145, \text{ ideally } 0.125,$$

$$z = 0.380, \text{ ideally } 0.375.$$

Some of the Mn are also displaced:

$$\text{Mn(2): } 24d\text{: } x = 0.970 = -0.030, \text{ instead of } 0.000.$$

e. I Complex. The 59 bcc structures are represented by the W structure type,

$$[W\ W\ W\ W].$$

Binary derivatives are:

CeH_3† [Ce H H H],

NaTl [Na Na Tl Tl]

CsCl [Cs Cl Cs Cl].

A distorted form of the CsCl structure is that of CoU. Eight unit cells of CsCl are needed to provide a CoU unit cell. The distortions along the body-diagonal directions:

for Co $x = y = z = 0.294$, ideally 0.25,

and for U $x = y = z = 0.0347$, ideally 0.00.

A special derivative of CsCl, CaB_6, is discussed under "special nets."

$AlCu_2Mn$ [Al Cu Mn Cu].

There are several superstructures of the bcc and CsCl structure types. Two of these are Al_4Cu_9 and Cu_5Zn_8. They can be derived from the CsCl structure by taking $3 \times 3 \times 3$ unit cells of CsCl, and distributing 52 atoms and two vacancies in an ordered fashion over the resulting 54 bcc lattice points. The occupancy of the

† Sometimes known as the BiF_3 structure, which, however, is controversial.

Cs- and Cl-type locations is as follows:

	Cs sites	Cl sites
Al_4Cu_9:	$(Al_{16/27}Cu_{10/27}Vac_{1/27})$	$(Cu_{26/27}Vac_{1/27})$
Cu_5Zn_8:	$(Zn_{16/27}Cu_{10/27}Vac_{1/27})$	$(Zn_{16/27}Cu_{10/27}Vac_{1/27})$.

Other ordered superstructures of the bcc lattice requiring 54 bcc lattice points per unit cell are Fe_3Zn_{10} and Sb_2Tl_7, which are analogous as follows:

$$4\ Fe_3Zn_{10} = Fe_{12}Zn_{40}Vac_2,$$
$$6\ Sb_2Tl_7 = Sb_{12}Tl_{40}Tl_2.$$

Finally, S_4Tl_3V can be considered a derivative of the CsCl structure type, although the S-V distance is considerably shortened with resulting distortion of the S array:

$$\begin{bmatrix} S & V & S & V \\ S & Tl & S & Tl \\ S & Tl & S & Tl \\ S & Tl & S & Tl \end{bmatrix}.$$

Distortion: S: $x = y = z = 0.175$, ideally 0.250.

f. One-Quarter and Three-Quarter Occupied *h* Planes. In the structures discussed so far *h* planes were either completely empty or completely occupied, albeit by more than one element. (Exceptions are those cases where a small fraction of sites is vacant.) Presently we consider the following structure types in which some *h* planes are partly occupied:

Cu_2O
$$\begin{bmatrix} Cu & Ox & 0 & Ox \\ Cu & 0 & 0 & 0 \\ Cu & 0 & 0 & 0 \\ Cu & 0 & 0 & 0 \end{bmatrix},$$

Hg_4Pt
$$\begin{bmatrix} Hg & Pt & Hg & Pt \\ Hg & 0 & Hg & 0 \\ Hg & 0 & Hg & 0 \\ Hg & 0 & Hg & 0 \end{bmatrix},$$

ReO_3
$$\begin{bmatrix} 0 & 0 & Re & 0 \\ Ox & 0 & 0 & 0 \\ Ox & 0 & 0 & 0 \\ Ox & 0 & 0 & 0 \end{bmatrix},$$

$CaTiO_3$
$$\begin{bmatrix} Ca & 0 & Ti & 0 \\ Ox & 0 & 0 & 0 \\ Ox & 0 & 0 & 0 \\ Ox & 0 & 0 & 0 \end{bmatrix},$$

CFe_4
$$\begin{bmatrix} Fe & C & 0 & 0 \\ Fe & 0 & 0 & 0 \\ Fe & 0 & 0 & 0 \\ Fe & 0 & 0 & 0 \end{bmatrix}.$$

Distortion: Fe: $x = y = z = 0.265$, ideally 0.250.

A large number of structure types contain half occupied *F* complexes. We have seen that a single hexagonal net cannot be symmetrically divided into two equivalent parts, but that one-half of the *F* complex can be symmetrically occupied by occupying respectively one-fourth and three-fourths of alternate *h* planes. The resulting array is the *T* complex, sometimes called the three-dimensional Kagomé net because it contains

Kagomé nets in the four directions perpendicular to the four body diagonals. The *T* complex was shown to be interstitial derivative of the *D* complex. The distribution matrix is a function of *h*-modulo-4 because of the different occupancy of alternate *h* planes in the fcc array. The following structure types all contain three-dimensional Kagomé nets.

Al_2MgO_4 (spinel)

$$\begin{bmatrix} Ox & Mg & Al & Mg & Ox & 0 & 0 & 0 \\ Ox & 0 & 0 & 0 & Ox & 0 & Al & 0 \\ Ox & 0 & 0 & 0 & Ox & 0 & Al & 0 \\ Ox & 0 & 0 & 0 & Ox & 0 & Al & 0 \end{bmatrix}.$$

The Mg's occupy a *D* complex.

Cu_2Mg (Laves phase)

$$\begin{bmatrix} 0 & Mg & Cu & Mg & 0 & 0 & 0 & 0 \\ 0 & 0 & 0 & 0 & 0 & 0 & Cu & 0 \\ 0 & 0 & 0 & 0 & 0 & 0 & Cu & 0 \\ 0 & 0 & 0 & 0 & 0 & 0 & Cu & 0 \end{bmatrix}.$$

(Observe that the cations in spinel form a Laves phase!)

$Ca_{33}Ge$

$$\begin{bmatrix} Ca & 0 & 0 & 0 & Ca & 0 & X & 0 \\ Ca & 0 & X & 0 & Ca & 0 & 0 & 0 \\ Ca & 0 & X & 0 & Ca & 0 & 0 & 0 \\ Ca & 0 & X & 0 & Ca & 0 & 0 & 0 \end{bmatrix},$$

where X = random mixture of Ca and Ge.

C_6Cr_{23}

$$\begin{bmatrix} \{Cr(1)Cr_{12}(3)\} & Cr(4) & Cr(2) & Cr(4) & 0 & 0 & Cr(2) & 0 \\ 0 & 0 & C & 0 & 0 & Cr(4) & C & Cr(4) \\ 0 & 0 & C & 0 & 0 & Cr(4) & C & Cr(4) \\ 0 & 0 & C & 0 & 0 & Cr(4) & C & Cr(4) \end{bmatrix}.$$

Twelve Cr(3)'s form a regular icosahedron around each Cr(1). Distortions: For C, $x = 0.275$, ideally 0.250; for Cr(4), $x = 0.385$, ideally 0.375.

$AuBe_5$

$$\begin{bmatrix} 0 & Be(1) & Be(2) & Au & 0 & 0 & 0 & 0 \\ 0 & 0 & 0 & 0 & 0 & 0 & Be(2) & 0 \\ 0 & 0 & 0 & 0 & 0 & 0 & Be(2) & 0 \\ 0 & 0 & 0 & 0 & 0 & 0 & Be(2) & 0 \end{bmatrix}$$

Note resemblance to Laves phase.

Cu_4S_4Sb

$$\begin{bmatrix} S & 0 & S & Sb & 0 & 0 & 0 & Sb \\ 0 & Cu & 0 & 0 & S & Cu & S & 0 \\ 0 & Cu & 0 & 0 & S & Cu & S & 0 \\ 0 & Cu & 0 & 0 & S & Cu & S & 0 \end{bmatrix}.$$

Al_2S_3

$$\begin{bmatrix} S & Al_{2/3}(1) & Al(2) & Al_{2/3}(1) & S & 0 & 0 & 0 \\ S & 0 & 0 & 0 & S & 0 & Al(2) & 0 \\ S & 0 & 0 & 0 & S & 0 & Al(2) & 0 \\ S & 0 & 0 & 0 & S & 0 & Al(2) & 0 \end{bmatrix}.$$

Co_9S_8

$$\begin{bmatrix} S(1) & Co(2) & Co(1) & Co(2) & S(1) & 0 & 0 & 0 \\ S(2) & 0 & 0 & 0 & S(2) & Co(2) & 0 & Co(2) \\ S(2) & 0 & 0 & 0 & S(2) & Co(2) & 0 & Co(2) \\ S(2) & 0 & 0 & 0 & S(2) & Co(2) & 0 & Co(2) \end{bmatrix}.$$

Distortions: S(2): $x = 0.2591$, ideally 0.2500; Co(2): $x = 0.1268$, ideally 0.1250.

E-$Al_{18}Cr_2Mg_3$

$$\begin{bmatrix} Mg(2) & 0 & 0 & \{Mg(1)Al_{12}(2)\} & Cr & \{Mg(1)Al_{12}(2)\} & 0 & 0 \\ Cr & Al(1) & 0 & Al(1) & Mg(2) & Al(1) & 0 & Al(1) \\ Cr & Al(1) & 0 & Al(1) & Mg(2) & Al(1) & 0 & Al(1) \\ Cr & Al(1) & 0 & Al(1) & Mg(2) & Al(1) & 0 & Al(1) \end{bmatrix}.$$

The Al(2) form truncated tetrahedra of equal edge lengths (Laves Polyhedra) around Mg(1). The side of these polyhedra is such that their hexagonal faces perpendicularly bisect line segments from Mg(1) to Mg(2). There is a very large distortion of the Al(1) array: $x = 0.1407$, ideally $x = 0.250$. The only justification for indexing Al(1) as is done here is that the only invariant lattice complex with multiplicity 48 is J_2^*, which has a distribution matrix as given for Al(1) above. Alternately, the Al's could be considered as octahedral clusters centered on a D complex (multiplicity 8). In that case, the distribution matrix would be:

$$\begin{bmatrix} \text{Mg(2)} & \text{Al}_6\text{(1)} & 0 & \{\text{Mg(1)Al}_{12}\text{(2)}\} & \text{Cr} & \{\text{Mg(1)Al}_{12}\text{(2)}\} & 0 & \text{Al}_6\text{(1)} \\ \text{Cr} & 0 & 0 & 0 & \text{Mg(2)} & 0 & 0 & 0 \\ \text{Cr} & 0 & 0 & 0 & \text{Mg(2)} & 0 & 0 & 0 \\ \text{Cr} & 0 & 0 & 0 & \text{Mg(2)} & 0 & 0 & 0 \end{bmatrix},$$

$\text{Mn}_{23}\text{Th}_6$

$$\begin{bmatrix} \text{Mn(3)} & 0 & \text{Mn(4)} & \text{Mn(1)} & \text{Mn(4)} & 0 & \text{Mn(3)} & 0 \\ \text{Mn(4)} & \text{Th} & \text{Mn(3)} & \text{Mn(2)} & \text{Mn(3)} & \text{Th} & \text{Mn(4)} & \text{Mn(2)} \\ \text{Mn(4)} & \text{Th} & \text{Mn(3)} & \text{Mn(2)} & \text{Mn(3)} & \text{Th} & \text{Mn(4)} & \text{Mn(2)} \\ \text{Mn(4)} & \text{Th} & \text{Mn(3)} & \text{Mn(2)} & \text{Mn(3)} & \text{Th} & \text{Mn(4)} & \text{Mn(2)} \end{bmatrix}.$$

The Mn(3) is distorted: $x = 0.178$, ideally 0.125,
Mn(4) : $x = 0.378$, ideally 0.375,
Th : $x = 0.203$, ideally 0.250.

These distortions are consistent with the substitution for Mn of three vacancies and six Th atoms per 32 Mn in a bcc array.

$\text{Cu}_{16}\text{Mg}_6\text{Si}_7$

$$\begin{bmatrix} \text{Cu(2)} & 0 & \text{Cu(1)} & \text{Si(1)} & \text{Cu(1)} & 0 & \text{Cu(2)} & 0 \\ \text{Cu(1)} & \text{Mg} & \text{Cu(2)} & \text{Si(2)} & \text{Cu(2)} & \text{Mg} & \text{Cu(1)} & \text{Si(2)} \\ \text{Cu(1)} & \text{Mg} & \text{Cu(2)} & \text{Si(2)} & \text{Cu(2)} & \text{Mg} & \text{Cu(1)} & \text{Si(2)} \\ \text{Cu(1)} & \text{Mg} & \text{Cu(2)} & \text{Si(2)} & \text{Cu(2)} & \text{Mg} & \text{Cu(1)} & \text{Si(2)} \end{bmatrix}.$$

This structure is closely related to that of $\text{Mn}_{23}\text{Th}_6$. Distortions: Cu(2): $x = 0.1684$, ideally 0.125, Cu(1): $x = 0.3770$, ideally 0.375, and Mg: $x = 0.1824$, ideally 0.250.

CFe_3W_3

$$\begin{bmatrix} \text{Fe(2)} & 0 & \text{Fe(1)} & 0 & \text{Fe(2)} & 0 & \text{C} & 0 \\ \text{Fe(2)} & \text{W} & \text{C} & \text{W} & \text{Fe(2)} & \text{W} & \text{Fe(1)} & \text{W} \\ \text{Fe(2)} & \text{W} & \text{C} & \text{W} & \text{Fe(2)} & \text{W} & \text{Fe(1)} & \text{W} \\ \text{Fe(2)} & \text{W} & \text{C} & \text{W} & \text{Fe(2)} & \text{W} & \text{Fe(1)} & \text{W} \end{bmatrix}.$$

Distortions: Fe(2): $x = 0.825$, ideally 0.875; W: $x = 0.195$, ideally, 0.250.

NiTi_2

$$\begin{bmatrix} \text{Ni} & 0 & \text{Ti(1)} & 0 & \text{Ni} & 0 & 0 & 0 \\ \text{Ni} & \text{Ti(2)} & 0 & \text{Ti(2)} & \text{Ni} & \text{Ti(2)} & \text{Ti(1)} & \text{Ti(2)} \\ \text{Ni} & \text{Ti(2)} & 0 & \text{Ti(2)} & \text{Ni} & \text{Ti(2)} & \text{Ti(1)} & \text{Ti(2)} \\ \text{Ni} & \text{Ti(2)} & 0 & \text{Ti(2)} & \text{Ni} & \text{Ti(2)} & \text{Ti(1)} & \text{Ti(2)} \end{bmatrix}.$$

Distortions: Ni: $x = 0.215$, ideally 0.250; Ti(2): $x = 0.810$, ideally 0.875.

$\alpha\text{-Al}_{13}\text{Cr}_4\text{Si}_4$

$$\begin{bmatrix} \text{Al(1)} & \text{Cr} & 0 & \text{Si} & 0 & 0 & 0 & 0 \\ \text{Al(3)} & 0 & \text{Al(2)} & 0 & \text{Al(3)} & \text{Cr} & \text{Al(2)} & \text{Si} \\ \text{Al(3)} & 0 & \text{Al(2)} & 0 & \text{Al(3)} & \text{Cr} & \text{Al(2)} & \text{Si} \\ \text{Al(3)} & 0 & \text{Al(2)} & 0 & \text{Al(3)} & \text{Cr} & \text{Al(2)} & \text{Si} \end{bmatrix}.$$

Distortions: Al(2): $x = 0.315$, ideally 0.250, and Al(3): $x = 0.565$, ideally 0.500 (distortion exactly $\frac{1}{16}$); Cr: $x = 0.342$, ideally 0.375.

Now follow structures in which linear arrays of atoms are centered on some points of the bcc lattice. Here, the orientation of the arrays must be given as well as the location of their geometrical centers. This is done by subscripts: 111, $1\bar{1}\bar{1}$, $\bar{1}1\bar{1}$, and $\bar{1}\bar{1}1$ indicate the four body-diagonal directions.

FeSi. The arrays are pairs of Fe and Si atoms which lie on opposite sides of points of the F complex: the lattice points are not occupied themselves. The array is denoted by (Fe□Si), where □ indicates the unoccupied lattice points. The pairs are oriented parallel to the four-body diagonals. The distribution matrix is:

$$\begin{bmatrix} (\mathrm{Fe}\square\mathrm{Si})_{111} & 0 & 0 & 0 \\ (\mathrm{Fe}\square\mathrm{Si})_{1\bar{1}\bar{1}} & 0 & 0 & 0 \\ (\mathrm{Fe}\square\mathrm{Si})_{\bar{1}1\bar{1}} & 0 & 0 & 0 \\ (\mathrm{Fe}\square\mathrm{Si})_{\bar{1}\bar{1}1} & 0 & 0 & 0 \end{bmatrix}.$$

FeS_2. The Fe atoms occupy an *F* complex. The S atoms form pairs centered on an *F* complex:

$$\begin{bmatrix} (\mathrm{S}\square\mathrm{S})_{111} & 0 & \mathrm{Fe} & 0 \\ (\mathrm{S}\square\mathrm{S})_{1\bar{1}\bar{1}} & 0 & \mathrm{Fe} & 0 \\ (\mathrm{S}\square\mathrm{S})_{\bar{1}1\bar{1}} & 0 & \mathrm{Fe} & 0 \\ (\mathrm{S}\square\mathrm{S})_{\bar{1}\bar{1}1} & 0 & \mathrm{Fe} & 0 \end{bmatrix}.$$

This is, therefore, a derivative of the NaCl structure, as is the following:

$$\begin{bmatrix} (\mathrm{S}\square\mathrm{Sb})_{111} & 0 & \mathrm{Ni} & 0 \\ (\mathrm{S}\square\mathrm{Sb})_{1\bar{1}\bar{1}} & 0 & \mathrm{Ni} & 0 \\ (\mathrm{S}\square\mathrm{Sb})_{\bar{1}1\bar{1}} & 0 & \mathrm{Ni} & 0 \\ (\mathrm{S}\square\mathrm{Sb})_{\bar{1}\bar{1}1} & 0 & \mathrm{Ni} & 0 \end{bmatrix}.$$

Here, there is a slight distortion of the Ni array from the idealized *F* complex: $x = 0.976$ ($= -0.024$), ideally 0.000. The reason is that each Ni is surrounded by one S and one Sb, whereas in FeS_2, the Fe atoms being surrounded by S atoms on both sides are located on an ideal *F* complex.

In both FeS_2 and NiSSb there is some arbitrariness about where the S pairs, respectively SSb pairs are centered. It would be conceivable also to pair the anions differently, so that triplets (S Fe S), respectively (Sb Ni S) would be centered on the Fe, respectively Ni sites. The determining factor is the interatomic distance:

Ni–S:	2.34 Å	Fe–S:	2.259 Å
Ni–Sb:	2.51 Å	S–S:	2.171 Å
Sb–S:	2.40 Å		

In the FeS_2 case, the S atoms are closest when paired through unoccupied fcc lattice sites. In NiSSb there is some latitude, though the Sb–S distance is smaller than the average of the NiS and NiSb distances.

The high-temperature Si III is also related to FeS_2. Here, pairs of Si atoms are centered on a primitive cubic complex, with orientations parallel to the body diagonals.

$$\begin{bmatrix} (\mathrm{Si}\square\mathrm{Si})_{111} & 0 & (\mathrm{Si}\square\mathrm{Si})_{111} & 0 \\ (\mathrm{Si}\square\mathrm{Si})_{1\bar{1}\bar{1}} & 0 & (\mathrm{Si}\square\mathrm{Si})_{1\bar{1}\bar{1}} & 0 \\ (\mathrm{Si}\square\mathrm{Si})_{\bar{1}1\bar{1}} & 0 & (\mathrm{Si}\square\mathrm{Si})_{\bar{1}1\bar{1}} & 0 \\ (\mathrm{Si}\square\mathrm{Si})_{\bar{1}\bar{1}1} & 0 & (\mathrm{Si}\square\mathrm{Si})_{\bar{1}\bar{1}1} & 0 \end{bmatrix}.$$

2. Special Equally Spaced Nets

Many of these structures also fit into the category just discussed, but permit more detailed description in the present category.

$$\mathrm{CaB_6}: \quad [\mathrm{CaB_6CaB_6}].$$

This is a structure of the CsCl type, with octahedra of B_6 occupying the Cl positions. The size of the B_6 octahedra is such that each Ca is surrounded by 24 B atoms at the vertices of a truncated cube whose edge lengths are all equal. The B atoms, therefore, form a three-dimensional net whose nodes are equally spaced.

For UB_{12}, data are given in an awkward manner. For proper identification of relevant patterns, it is well to change the notation as follows: The U atoms form an F complex at locations $0\,0\,0 + \frac{1}{2}\,\frac{1}{2}\,0_{\mathcal{F}}$. The locations of 48 B atoms per unit cell are commonly given as

$$(0\,0\,0, \tfrac{1}{2}\,\tfrac{1}{2}\,0_{\mathcal{F}}) + (\tfrac{1}{2}, \pm x, \pm x)_{\mathcal{F}},$$

where $x = 0.167 \doteq \frac{1}{6}$.
Since

$$\tfrac{1}{2}\,\tfrac{1}{6}\,\bar{\tfrac{1}{6}} + \tfrac{1}{2}\,0\,\tfrac{1}{2} \overset{1}{=} 0\,\tfrac{1}{6}\,\tfrac{1}{3},$$

$$\tfrac{1}{2}\,\bar{\tfrac{1}{6}}\,\tfrac{1}{6} + \tfrac{1}{2}\,\tfrac{1}{2}\,0 \overset{1}{=} 0\,\tfrac{1}{3}\,\tfrac{1}{6},$$

$$\tfrac{1}{2}\,\bar{\tfrac{1}{6}}\,\bar{\tfrac{1}{6}} + \tfrac{1}{2}\,\tfrac{1}{2}\,0 \overset{1}{=} 0\,\tfrac{1}{3}\,\tfrac{1}{6},$$

$$\tfrac{1}{2}\,\tfrac{1}{6}\,\tfrac{1}{6} + \tfrac{1}{2}\,\bar{\tfrac{1}{2}}\,0 \overset{1}{=} 0\,\bar{\tfrac{1}{3}}\,\tfrac{1}{6}, \quad \text{etc.},$$

these 48 points are more conveniently described as:

$$(0\,0\,0, 0\,\tfrac{1}{2}\,\tfrac{1}{2}_{\mathcal{F}}) + (0, \pm\tfrac{1}{6}, \pm\tfrac{1}{3})_{\mathcal{F}}.$$

This means that each U atom is surrounded by 24 B atoms at the corners of a truncated octahedron with equal edges (the "Domuledron" shape). These truncated octahedra share edges, so that the boron atoms form a three-dimensional net with equally spaced nodes.

To visualize the space between the truncated octahedra, note that truncated octahedra, cuboctahedra, and truncated tetrahedra, all of equal edge lengths, together can fill space. Each truncated octahedron shares its six square faces with six cuboctahedra and its eight hexagonal faces with eight truncated tetrahedra. Each truncated tetrahedron shares its four hexagonal faces with four truncated octahedra and its four triangular faces with four cuboctahedra. Each cuboctahedron shares its six square faces with six truncated octahedra and its eight triangular faces with eight truncated tetrahedra. The boron net of UB_{12} can, therefore, be thought of as having cuboctahedral, truncated tetrahedral, and truncated octahedral interstices, in ratio 1:2:1, of which all truncated octahedral ones are occupied by U atoms, which consequently form an *F* complex. The UB_{12} structure can be described by the following algorisms:

The atoms occupy *h* nets on the basis of the value of $(v - 2h)_{\text{mod } 9}$ and $(w - 2h)_{\text{mod } 9}$ (cf. Fig. 18).

		$h_{\text{mod}6}\rightarrow$					
		0	1	2	3	4	5
	00	U	0	0	0	0	0
	03	0	0	0	B	0	0
	06	0	0	0	B	0	0
	30	0	0	0	B	0	0
$(v-2h)_9, (w-2h)_9$	33	0	B	0	0	0	0
$\downarrow$	36	0	B	0	B	0	B
	60	0	0	0	B	0	0
	63	0	B	0	B	0	B
	66	0	0	0	0	0	B.

Alternately, a distribution matrix can be given that does not give detail for the B_{12} cuboctahedra, but stresses the relative positions of the centers of these cuboctahedra and the uranium atoms:

$$[\text{U } 0\ B_{12}\ 0].$$

Viewed in this manner, UB_{12} is a derivative of the NaCl structure.

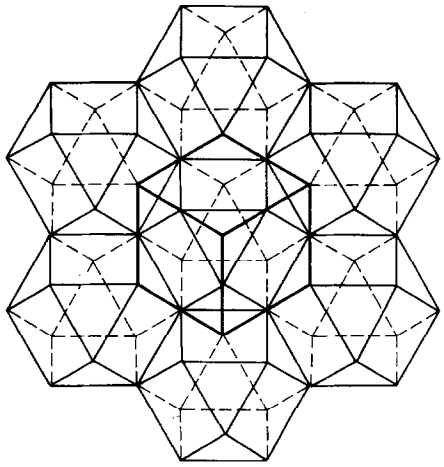

FIG. 18. Partial occupancy of hexagonal nets by B atoms in UB_{12}: the cuboctahedra are shown explicitly.

Another example of a special three-dimensional net is C_3Pu_2, which represents eleven structures having the general chemical formula C_3M_2, where M is a rare earth metal or lanthanum. The metal atoms here form a distorted ($x = 0.050$, ideally 0.000) *I* complex, the distortion being along a body-diagonal direction. The C atoms join pairs of metal atoms such that (MCM) triplets are linear. From each metal atom, three bonds go in mutually perpendicular directions through carbon atoms to other atoms, according to the following scheme:

Metal atom joined through	C	to	Metal atom
0 0 0	0 0 $\frac{3}{4}$		0 0 $\frac{1}{4}$
$\frac{1}{4}$ $\frac{1}{4}$ $\frac{1}{4}$	$\frac{1}{4}$ $\frac{1}{4}$ 0		$\frac{1}{4}$ $\frac{1}{4}$ $\frac{3}{4}$
$\frac{1}{2}$ $\frac{1}{2}$ $\frac{1}{2}$	$\frac{1}{2}$ $\frac{1}{2}$ $\frac{1}{4}$		$\frac{1}{2}$ $\frac{1}{2}$ 0
$\frac{3}{4}$ $\frac{3}{4}$ $\frac{3}{4}$	$\frac{3}{4}$ $\frac{3}{4}$ $\frac{1}{2}$		$\frac{3}{4}$ $\frac{3}{4}$ $\frac{1}{4}$
	etc.		

The distortion from the idealized bcc array would appear due to the C–M bonding.

Somewhat similar is the $CoAs_3$ structure. Here, the Co atoms form a *P* complex. Each Co is joined to its six nearest Co neighbors by a bond through an As atom; the Co–As–Co path is not a straight line, however, but subtends an angle of 120° at the As atom. Co–As–Co bonds lie in (110) planes. The As atoms accordingly occupy vertices of regular octahedra around the Co atoms, but these octahedra are skew-oriented within the cubical unit cell.

Next come several structures based on icosahedral coordination. The icosahedron is regular when $x = 0.62$. However, because of the impossibility of placing two five-fold axes parallel to each other, the icosahedron cannot be stacked and maintain its five-fold symmetry in its context, and is frequently distorted. However, its cubic symmetry (the regular icosahedron has cubic *plus* five-fold symmetry) is maintained; the distortions are such that the triangles of Fig. 14 always remain perpendicular to the cube diagonals.

The first of these structures based on icosahedral coordination is $NaZn_{13}$, a derivative of the CsCl structure having a distribution matrix

$$[Na\{Zn(1)Zn_{12}(2)\}Na\{Zn(1)Zn_{12}(2)\}].$$

The Zn(2) form icosahedra around the Zn(1). These icosahedra are almost, but not quite, regular having $x = 0.66$ instead of the ideal $x = 0.62$. The distances between Zn(2) atoms on adjacent icosahedra are nearly the same as those on the same icosahedron; distances from a Zn(2) to its nine near neighbor Zn(2) atoms are in the ratios 1:1.04:1.08:1.14, there being respectively two nearest, two next nearest, and four next-next nearest neighbors.

The icosahedra have two-fold, but not four-fold rotational symmetry. They orient themselves in two different, mutually perpendicular directions around their two-fold axes, adjacent icosahedra always being oriented perpendicularly. The sodium atoms are at the centers of cubes whose vertices are the centers of the icosahedra. An icosahedron turns regular triangular faces toward the sodium atoms; each sodium atom is accordingly surrounded by 24 Zn(2) atoms, which form the vertices of a so-called snub cube.

For $Al_{12}W$ the distribution matrix is:

$$[(WAl_{12})(WAl_{12})(WAl_{12})(WAl_{12})].$$

This means that groups of (WAl_{12}) are centered on an *I* complex. Each W is surrounded by 12 Al atoms at the vertices of a nearly regular icosahedron: $x = 0.595$ ideally 0.62. The icosahedra face each other with equilateral triangles in antiprism orientation perpendicular to body diagonals of the cubic unit cell. The Al atoms form a nearly equally spaced net. Distances of near neighbors are in the ratios 1:1.005:1.03:1.04.

3. Interstitial Derivatives of the *I* Complex

The parent structure type of this family is Cr_3O("*β-W*") which represents 67 different structures. The oxide ions occupy an *I* complex and the Cr ions occupy one-half of the interstices, i.e., a *W* complex. We have noted that *β*-UH_3 and $AuZn_3$(L.T.) may be considered interstitial derivatives of the *β-W* structure.

GeK: The Ge atoms form tetrahedral Ge clusters centered on a *β-W* structure (*I* + *W* complexes). Three-quarters of the K are located near interstices in *β-W*: $x = 0.336$, $y = 0.142$, $z = 0.064$, ideally $x = 0.313$, $y = 0.156$, $z = 0.00$. The remaining K are located at the corners of cubes around the Ge_4 clusters.

Ge_7Ir_3: These structures are quite idiosyncratic. Ge(1) occupies a *W** complex, whereas Ir forms octahedra around a bcc complex and the Ge(2) form cubes around the same bcc complex.

$Cu_{15}Si_4$: The Si atoms form a distorted *I* complex: $x = y = z = 0.208$, ideally 0.250. Cu(1) forms an S^+ complex in the interstices. Cu(2) occupies a variable complex 143*d*48(*e*) $x = 0.12$, $y = 0.16$, $z = 0.96$, which does not appear to fit any significant pattern.

Other structures in which the *I* and *W* complexes occur together are:

Ag_3AuTe_2: The Te atoms occupy a slightly distorted *I* complex: $x = 0.266$, ideally 0.250. This distortion is due to the asymmetrical environment of Ag atoms, which occupy one-fourth of the interstices, in an *S** complex. The Au ions occupy a $^+Y^*$ complex, a partial occupancy of the hexagonal net (cf. *α*-In_2Te_3, Section L under 1b.)

P_4Th_3: The Th atoms occupy an ^+S complex, one-eighth of all interstices in a bcc complex. The P atoms occupy the equipoints given in the International Tables as I43d, 16(c). This set of equipoints is a variable complex; for P_4Th_3 $x = y = z = 0.083$. With $x = 0$ this complex becomes an *I* complex, but with $x = \frac{1}{8}$ it becomes *Y***. In view of the role of $^+$S as a distribution over interstices in an *I* complex, it is most logical to consider the array of P atoms as an, albeit strongly distorted, *I* complex.

Ce_2S_3: A defect structure of P_4Th_3 which could, for the sake of analogy, be written $S_4(Ce_{8/9}Vac_{1/9})_3$.

4. The Mn Structures

Both *α*-Mn and *β*-Mn have defied a structural classification. *β*-Mn and Al_2CMo_3 are closely related: Mn(1) is analogous to Al, Mn(2) to Mo, with the *C* sites in Al_2CMo_3 being unoccupied in *β*-Mn. The Mn(1), respectively Al occupy a distorted ($x = 0.061$ i.s.o. ideally 0.00) *D* complex. The structure of *α*-Mn is altogether idiosyncratic. The complicated structures of the Brillouin zones of Mn are probably responsible for these complex structures that do not fit a simple geometrical model, but represent various balances and compromises.

5. Miscellaneous Idiosyncratic Structures

Other structures that are too complex to fit a simple geometric model are: $Cu_{12}S_{13}Sb_4$, $(Al, Zn)_{49}Mg_{32}$, $Pd_{17}Se_{15}$, $Be_{17}Ru_3$, $Li_{22}Pb_5$, $BaHg_{11}$, Bi_4Rh, and Mg_2Zn_{11}.

These structures do not seem to relate in any way to each other or to any other structures.

Acknowledgments

Much of the work reported here constitutes part of a project undertaken jointly with Dr. W. B. Pearson attempting the development of a systematic atlas of metal phases. The author is indebted to Dr. Pearson for supplying a great many data for classification.

References

1. A. L. Loeb, *Acta Cryst.* **17**, 179 (1964).
2. M. O. Figueiredo (to be published).
3. A. L. Loeb, *Acta Cryst.* **11**, 469 (1958).
4. A. L. Loeb, *Acta Cryst.* **15**, 219 (1962).
5. F. Jellinek, *Oesterr. Chemiker. Z.* **60**, 311 (1959).
6. I. L. Morris and A. L. Loeb, *Acta Cryst.* **13**, 434 (1960).
7. W. G. Gehman, *J. Chem. Fed.* **40**, 54 (1963).
8. W. G. Gehman, *Acta Cryst.* **17**, 1561 (1964).
9. W. G. Gehman and S. B. Austerman, *Acta Cryst.* **18**, 375 (1965).
10. J. Lima-de-Faria, *Z. Krist.* **122**, 346 (1965).
11. J. Lima-de-Faria, *Z. Krist.* **122**, 359 (1965).
12. N. L. Smirnova, *Acta Cryst.* **21**, A33 (1966).
13. R. B. Fuller, A. L. Loeb, et al. (Peter Pearce, Ed.) (to be published, Macmillan).
14. F. Laves, *Trans. Amer. Soc. Metals* **48A**, 124 (1956).
15. F. C. Frank and J. S. Kasper, *Acta Cryst.* **11**, 184 (1958).
16. F. C. Frank and J. S. Kasper, *Acta Cryst.* **12**, 483 (1959).
17. E. W. Gorter, "Anorganische Chemie," p. 303, Butterworths, London, 1960.
18. W. B. Pearson, "Handbook of Lattice Spacings and Structures of Metals," Vol. 2, Pergamon Press, London/New York, 1967.
19. E. Hellner, *Acta Cryst.* **19**, 703 (1965).
20. J. D. H. Donnay, E. Hellner, and A. Niggli, *Z. Krist.* **123**, 255 (1966).
21. H. Burzlaff, W. Fischer, and E. Hellner, *Acta Cryst.* **A24**, 57 (1968).
22. A. L. Loeb and G. W. Pearsall, *Amer. J. Phys.* **31**, 190 (1963).